nature communications

Article

https://doi.org/10.1038/s41467-024-51414-6

Highly potent and broadly neutralizing anti-CD4 trimeric nanobodies inhibit HIV-1 infection by inducing CD4 conformational alteration

Received: 30 October 2023

Accepted: 6 August 2024

Published online: 13 August 2024

Check for updates

Linjing Zhu[1,2,3,16], Bilian Huang[1,16], Xiangyao Wang[4,16], Fengfeng Ni[5,6,16], Mingjun Ao[7,16], Ruoke Wang[8], Bin Zheng[7], Chen Chen[9], Jing Xue[10], Lin Zhu[10], Chenbo Yang[10], Lingen Shi[1], Shengya Geng[1,11], Jiaqian Hu[1], Mengshi Yang[5], Doudou Zhang[1], Ping Yang[5], Miaomiao Li[5,6], Yuncheng Li[5,6], Qinxue Hu[5], Sheng Ye[4,12], Peng Zheng[7], Hongxia Wei[9], Zhiwei Wu[1,2,13,14] ✉, Linqi Zhang[8] ✉, Yaxin Wang[4] ✉, Yalan Liu[5,15] ✉ & Xilin Wu[1,2,14] ✉

Despite advancements in antiretroviral therapy (ART) suppressing HIV-1 replication, existing antiviral drugs pose limitations, including lifelong medication, frequent administration, side effects and viral resistance, necessitating novel HIV-1 treatment approaches. CD4, pivotal for HIV-1 entry, poses challenges for drug development due to neutralization and cytotoxicity concerns. Nevertheless, Ibalizumab, the sole approved CD4-specific antibody for HIV-1 treatment, reignites interest in exploring alternative anti-HIV targets, emphasizing CD4's potential value for effective drug development. Here, we explore anti-CD4 nanobodies, particularly Nb457 from a CD4-immunized alpaca. Nb457 displays high potency and broad-spectrum activity against HIV-1, surpassing Ibalizumab's efficacy. Strikingly, engineered trimeric Nb457 nanobodies achieve complete inhibition against live HIV-1, outperforming Ibalizumab and parental Nb457. Structural analysis unveils Nb457-induced CD4 conformational changes impeding viral entry. Notably, Nb457 demonstrates therapeutic efficacy in humanized female mouse models. Our findings highlight anti-CD4 nanobodies as promising HIV-1 therapeutics, with potential implications for advancing clinical treatment against this global health challenge.

Although antiretroviral therapy (ART) has been efficacious in controlling HIV-1 replication over extended periods, it is not a curative treatment and requires lifelong administration[1]. The emergence of HIV-1 drug resistance has become increasingly prevalent, with untreated patients experiencing an estimated 7–19% prevalence of resistance to non-nucleoside reverse transcriptase inhibitors (NNRTIs) (known as transmitted drug resistance) and a much higher prevalence of 50–80% for NNRTIs in patients who have received ART[2,3]. Hence, potent broadly neutralizing antibodies (bNAbs) have emerged as a promising alternative or complementary approach for HIV-1 immunotherapy[4]. Nevertheless, bNAbs targeting the HIV-1 envelope spike may be susceptible to antibody resistance, potentially limiting

A full list of affiliations appears at the end of the paper. ✉e-mail: wzhw@nju.edu.cn; zhanglinqi@tsinghua.edu.cn; wangyaxin@tju.edu.cn; liuyl@wh.iov.cn; xilinwu@nju.edu.cn

their clinical efficacy[5]. In contrast, CD4, which serves as the primary host receptor for HIV-1 entry, represents a promising target for HIV-1 treatment. However, antibodies targeting CD4 with potent neutralization and low cytotoxicity are rare and thus only one such a drug is currently available in the market. Ibalizumab, a humanized IgG4 antibody targeting CD4, was approved as the pioneering antibody drug for the treatment of multidrug-resistant HIV-1 by the FDA in 2018[6,7]. Compared to traditional chemical drugs, Ibalizumab can be administered at long intervals, with a dosing frequency of once every 14 days[6,7]. In addition, we previously engineered a single-gene-encoded bispecific broadly neutralizing antibody, BiIA-SG, by combining two single-chain variable fragment (scFv) binding domains of Ibalizumab and a broadly neutralizing antibody, PGT-128, which targets HIV-1 gp120[8]. BiIA-SG demonstrated substantial improvements in breadth and potency, leading to functional cure in humanized mouse and macaque models, thereby highlighting the value of CD4 antibodies for the development of therapeutics against HIV-1[8,9].

Although Ibalizumab holds promise as an HIV-1 treatment, its clinical efficacy is limited by its relatively limited breadth and potency, which may lead to the emergence of viral escape during treatment. Additionally, Ibalizumab is a humanized monoclonal antibody derived from mice, which may have a high degree of immunogenicity during long-term administration. In addition, the high production costs associated with Ibalizumab may present a substantial obstacle to its long-term clinical use, which could limit its broad adoption.

Nanobodies have garnered significant interest in the development of drugs, given their advantages and potentials over traditional antibodies. Derived from the Camelidae family, nanobodies constitute the smallest naturally functional antibody fragment available to date[10–13], making it possible to create multi-targeted antibodies. Furthermore, nanobodies exhibit exceptional stability, even when administered subcutaneously[14]. Our previous results indicated that nanobody remained 100% activity even after prolonged exposure to high temperatures, such as 70 °C for an hour, and room temperature for two months, or after five rounds of repeated freezing and thawing[15,16]. In addition, recent findings have demonstrated that nanobodies can be efficiently produced in yeast, reducing the production cost considerably[12]. Importantly, our data, as well as other reports, indicated that nanobodies offered a unique binding mode to target proteins when compared to traditional antibodies, leading to remarkably potent neutralization against viral infections[16–18]. Following the approval of Caplacizumab, the first camel-derived nanobody, for marketing in 2018[19], numerous nanobodies currently have been in clinical trials including ALX-0651 for tumors, ALX-0171 for RSV virus, and ALX for inflammation[12,13,20], underscoring the significant therapeutic potential of nanobodies. Thus far, anti-CD4 nanobodies have been developed and utilized for in vivo CD4 cell tracing[21], while no anti-CD4 nanobodies have yet been developed for the therapeutic purpose of neutralizing HIV-1 infection.

The present study reported the isolation of anti-CD4 nanobodies from an alpaca immunized with human CD4 protein. Following the isolation, the nanobodies were characterized and evaluated for their ability to neutralize HIV-1 infection using a panel of 93 different viral strains. One broadly neutralizing nanobody, Nb457, was identified and subjected to structural analysis. The findings from the crystal structure analysis revealed that the binding of Nb457 induced the alteration of CD4's conformation, which impaired HIV-1 gp120 binding to CD4, thus preventing viral entry into host cells. Moreover, the anti-HIV activity of Nb457 or Nb457-based trimeric nanobodies was evaluated in a humanized mouse model. The results offered evidence that Nb457 exhibited exceptional potency against diverse HIV-1 genotypes without discernible cytotoxicity. The study calls for the development of Nb457-based nanobody drug for HIV-1 treatment.

Results

CD4-induced anti-sera potently inhibited HIV-1 pseudovirus

The high-titer anti-sera obtained from the third and fourth immunizations, with titers of 3.6×10^5 and 1.1×10^6, respectively, indicated that CD4-rFc was capable of inducing a strong immune response in the alpaca after the fourth immunization (Fig. 1a–c). To assess the neutralizing activity of the anti-sera against HIV-1 infection, a panel of diverse HIV-1 pseudovirus strains representing different subtypes that were isolated from both chronic and acute stages of infection were selected for neutralization assay. Following the fourth immunization, the anti-sera (4th anti-sera) demonstrated potent neutralizing activity against all 13 representative HIV-1 pseudoviruses, with an average 50% inhibitory dilution (ID_{50}) value of 9165, and neutralized 12 out of 13 pseudoviruses, achieving an average 90% inhibitory dilution (ID_{90}) value of 931 (Fig. 1d, e). These results suggest that the CD4-induced anti-sera possess broad and potent neutralizing activities against HIV-1 infection, thus providing a foundation for the subsequent isolation of anti-CD4 neutralizing nanobodies.

The isolation and characterization of anti-CD4 nanobodies

To isolate anti-CD4 nanobodies, a phage library displaying nanobodies was constructed from peripheral blood mononuclear cells (PBMC) obtained from the final immunization. The phage library had a diversity and in-frame rate exceeding 90%, and a size of 1.6×10^9, indicating high-quality establishment (Supplementary Fig. 1a). The CD4-his protein was utilized to enrich the library for three rounds, and single phage clones were selected from the enriched library for phage ELISA testing (Supplementary Fig. 1b). Results indicated that 30 out of 40 and 41 out of 46 clones were positive binders in the second and third enriched libraries, respectively, validating the enrichment process (Supplementary Fig. 1c). Consequently, a bacterial library was constructed based on the enriched phage library to obtain secreted nanobodies for characterization. Among 1920 single clones picked, 429 were positive binders on ELISA (Fig. 2a). Notably, 47 of these binders displayed neutralization activity against HIV-1 infection (Fig. 2b). Sequence alignment of the 429 positive binders and the 47 neutralizers revealed high diversity in the positive binders (Fig. 2c and Supplementary Fig. 1d).

To further characterize the anti-CD4 nanobodies, we expressed them in 293 F cells in the VHH-fused human Fc4 format (Fig. 2d). Notably, 29 out of 47 cell supernatants were able to bind to CD4 and effectively neutralize over 50% of HIV-1 infection (Fig. 2e, Supplementary Fig. 2 and Supplementary Table 1). Furthermore, 31 of the nanobodies exhibited affinities in the nanomolar range when measured for their binding affinity to CD4 (Fig. 2f and Supplementary Table 1). Based on these results and sequence analysis, we purified five nanobodies with distinct sequences (Nb_{319}-Fc, Nb_{434}-Fc, Nb_{457}-Fc, Nb_{505}-Fc, and Nb_{606}-Fc) for further evaluation of their neutralizing activity against representative HIV-1 pseudoviruses. Of these, Nb_{434}-Fc and Nb_{457}-Fc were found to be the most effective based on their neutralizing curve (Fig. 2g). SDS-PAGE analysis showed that Nb_{434}-Fc and Nb_{457}-Fc were of high purity (Supplementary Fig. 3a), and they were observed to preferentially bind to native CD4 protein in non-reduced conditions, indicating their interaction with a conformational epitope (Supplementary Fig. 3b). The binding curves of Nb_{457}-Fc and the reference antibody Ibalizumab in the Fc4 format were similar, with EC_{50} values of ~0.5 μg/ml, outperforming Nb_{434}-Fc with an EC_{50} value of 1.899 μg/ml (Supplementary Fig. 4).

Furthermore, these nanobodies were also found to recognize human CD4 cells, both on the spleen of humanized NDG-HuPBL mice, as observed through immunofluorescence staining (Supplementary Fig. 5), and in PBMC obtained from healthy donors, as assessed by flow cytometry (Supplementary Fig. 6). In order to elucidate the binding kinetics of these nanobodies with CD4, Bio-

https://doi.org/10.1038/s41467-024-51414-6

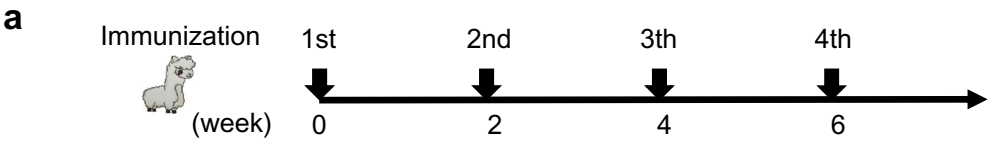

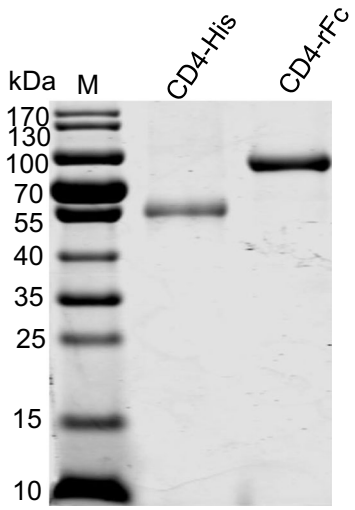

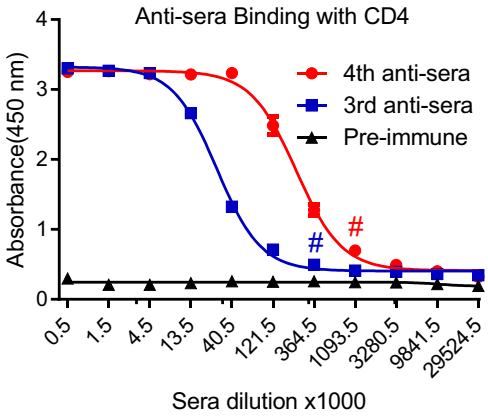

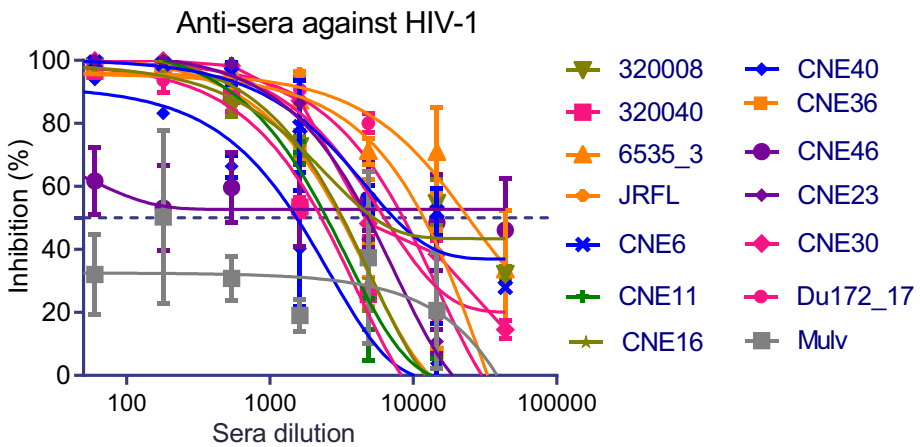

e

Virus	Subtype	Year of Isolation	Infection stage	R5 or X4	Risk factor	ID_{50}(dilution ratio)		ID_{90}(dilution ratio	
						Anti-sera	NC	Anti-sera	NC
320008	01AE	2009	Acute T/F	R5	MSM	18524	<20	350	<20
320040	01AE	2009	Acute T/F	R5	MSM	1861	<20	457	<20
6535_3	B	1995	Acute T/F	R5	IDU	27026	<20	1189	<20
JRFL	B	1986	chronic	R5	MSM	16421	<20	1828	<20
CNE6	B'	2006	chronic	R5	IDU	15995	<20	779	<20
CNE11	B'	2005	Chronic	R5	Blood	2436	<20	771	<20
CNE16	B'C	2007	chronic	R5	IDU	2963	<20	776	<20
CNE40	07_BC	2007	chronic	R5	IDU	1078	<20	90	<20
CNE36	08_BC	2007	chronic	R5	IDU	2737	<20	753	<20
CNE46	08_BC	2007	chronic	R5	IDU	13037	<20	<20	<20
CNE23	08_BC	2007	chronic	R5	IDU	4102	<20	1187	<20
CNE30	08_BC	2007	chronic	R5	IDU	4623	<20	1235	<20
Du172_17	C	1998	chronic	R5	?	8347	<20	1764	<20
Mulv	No HIV					<20	<20	<20	<20

Fig. 1 | Characterization of CD4-induced anti-sera in an alpaca. a Experimental schedule of immunization. **b** Detection of CD4 protein with His tag (CD4-His) or rabbit Fc tag (CD4-rFc) by SDS-PAGE. **c** Evaluation of anti-sera titer after the 3rd and 4th immunization in an alpaca receiving CD4-rFc protein. The *y*-axis represents the absorbance at 450 nm, and the x-axis shows the anti-sera dilution fold. Anti-sera binding with CD4-His are labeled on the graph. The terms "3rd anti-sera" (blue line) and "4th anti-sera"(red line) refer to the anti-sera collected one week after the 3rd and 4th immunizations, respectively. "Pre-immune" (black line) refer to the sera from alpaca before immunization, which was taken as negative control. # represents the antiserum titer. **d** Neutralizing curve of the 4th anti-sera against the panel of 13 HIV-1 pseudoviruses of various subtypes. Mulv served as the control virus. **e** Summary of 50% inhibitory dilution (ID_{50}) and 90% inhibitory dilution (ID_{90}) values, along with the information of pseudoviruses tested in the neutralization assay presented in panel **d**. Data for (**c**) and (**d**) are depicted as mean ± SEM. Source data are provided as a Source Data file.

https://doi.org/10.1038/s41467-024-51414-6

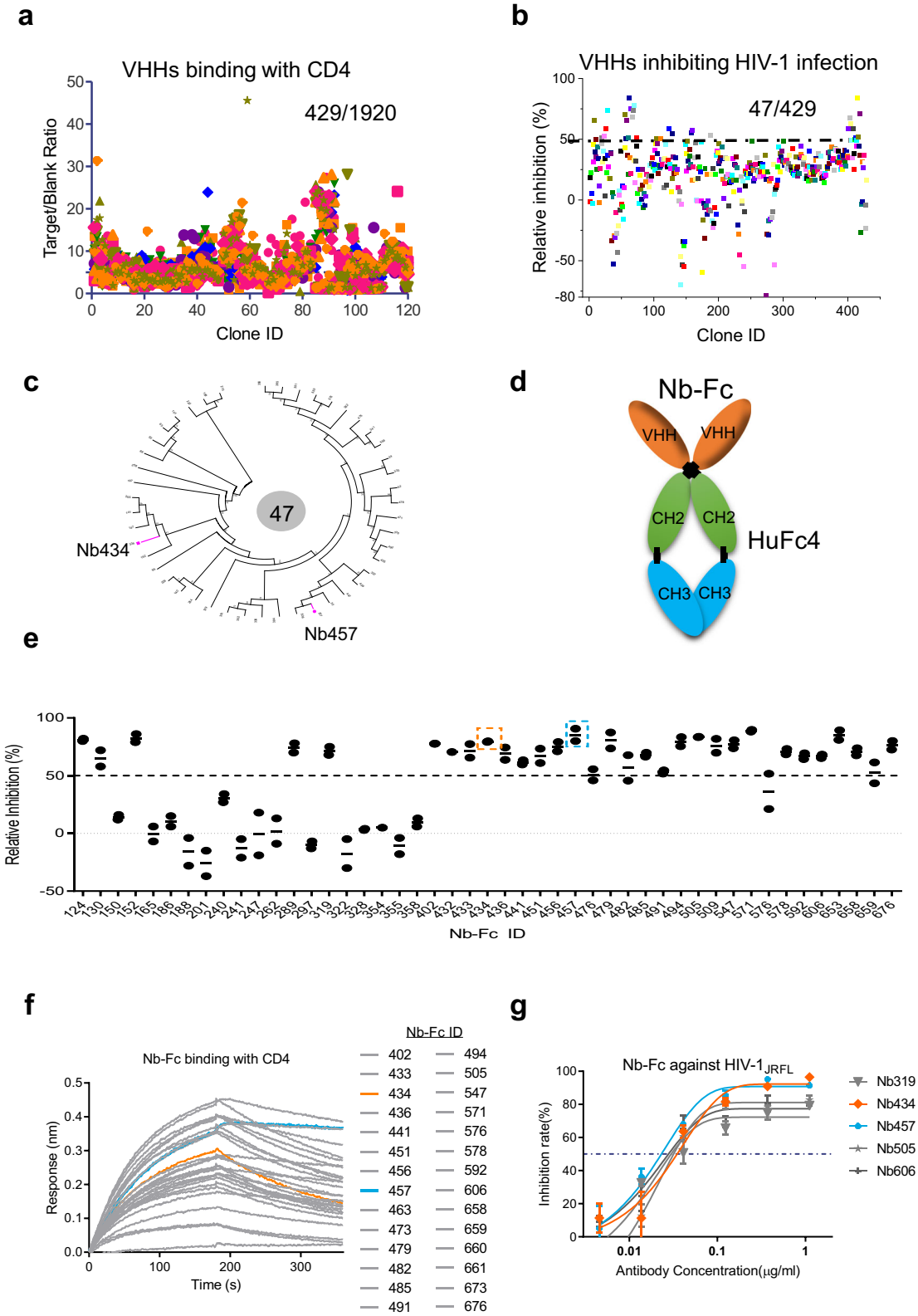

Layer Interferometry (BLI) was employed as the analytical method. The equilibrium dissociation constants (KD) for Nb_{434}-Fc, Nb_{457}-Fc, and Ibalizumab were 0.216 nM, 0.026 nM, and < 0.001 nM, respectively. Furthermore, the association constants (Ka) for Nb_{434}-Fc, Nb_{457}-Fc, and Ibalizumab were measured as $1.64 \times 10^7\ M^{-1}s^{-1}$, $2.89 \times 10^7\ M^{-1}s^{-1}$, and $1.2 \times 10^6\ M^{-1}s^{-1}$, respectively (Supplementary Fig. 7a–d).

Nb_{434}-Fc and Nb_{457}-Fc broadly neutralized HIV-1 infection in vitro

To evaluate the neutralizing activity of the anti-CD4 nanobodies Nb_{434}-Fc and Nb_{457}-Fc, we conducted analysis using a panel of 35 HIV-1 pseudoviruses that included isolates from multiple clades, covering major global HIV-1 subtypes CRF01_AE, B, B', CRF07_BC, CRF08_BC, B'C and C. This panel comprised 16 acute or transmitted/founder viruses

Fig. 2 | Isolation and characterization of anti-CD4 Nbs. a Summary of bacterial supernatant binding with CD4 protein tested by phage ELISA. The y-axis represents the ratio of the CD4 binding readout to the blank binding readout. Each dot corresponds to the bacterial supernatant from a single clone among the 1920 clones tested. **b** Positive binding VHHs inhibiting HIV-1 infection. Each dot represents one VHH clone supernatant. The dashed line indicates 50% relative inhibition. **c** Phylogenetic analysis of the 47 VHHs using the Neighbor-Joining method. The tree is drawn to scale, and branch lengths correspond to the evolutionary distances measured in amino acid substitutions per site. Evolutionary analyses were conducted using the Poisson correction method, with gaps and missing data excluded. MEGA6 software was utilized for the analyses. **d** Schematic diagram illustrating the structures of Nb-Fc (VHH fused with the Fc region), where the VHH is linked to the human Fc4 region (CH2–3). **e** Graph depicting the relative inhibition of cell supernatant from 47 various Nb-Fcs tested for neutralization against pseudovirus HIV-$1_{JR\text{-}FL}$ infection. The dashed line represents 50% inhibition. **f** Binding curves of 28 Nbs exhibiting interactions with the CD4 protein, as identified by BLI (Biolayer Interferometry), among the 47 various Nbs. **g** Neutralizing curve of the five selected Nbs against reference pseudoviruses of HIV-$1_{JR\text{-}FL}$. Data for (**g**) are depicted as mean ± SEM. Source data are provided as a Source Data file.

and 19 viruses isolated from chronic infections (Supplementary Table 2). Since nanobodies fused with Fc (~80 kDa) have smaller molecular weights than regular antibodies like Ibalizumab (~150 kDa), we compared the equimolar concentration (nM) of each and showed that both Nb_{434}-Fc (with median IC_{50} and IC_{90} values of 0.11 nM and 0.8 nM, respectively) and Nb_{457}-Fc (with median IC_{50} and IC_{90} values of 0.05 nM and 0.33 nM, respectively) were significantly more effective than Ibalizumab (with median IC_{50} and IC_{90} values of 0.15 nM and 26.145 nM, respectively) (Fig. 3a, b).

Overall, all three antibodies demonstrated substantial inhibitory activity, attaining 50% neutralization in all tested pseudoviruses (Fig. 3a and Supplementary Table 2). Intriguingly, Nb_{434}-Fc and Nb_{457}-Fc achieved 90% inhibition of infection in 100% and 91.4% of tested pseudoviruses, respectively, compared to Ibalizumab, which achieved 90% inhibition of infection in only 54.2% of tested pseudoviruses (Fig. 3b and Supplementary Table 2). Furthermore, we found that all 17 Ibalizumab-resistant pseudoviruses could be neutralized by Nb_{434}-Fc, and 14 out of 17 Ibalizumab-resistant pseudoviruses could be neutralized by Nb_{457}-Fc (Fig. 3c and Supplementary Table 2). Additionally, we observed that these three antibodies exhibited varied potency against different subtypes of HIV-1 pseudovirus (Fig. 3d–f and Supplementary Fig. 8a–c). For example, Ibalizumab failed to neutralize all the tested B'C viruses with 90% inhibition, while Nb_{434}-Fc and Nb_{457}-Fc neutralized 100% and 50% of them, respectively, with an IC_{90} value of <1 nM (Fig. 3d–f). Furthermore, Ibalizumab neutralized only 25% of tested subtype AE viruses with an IC_{90} value of 10 nM-100 nM, while Nb_{434}-Fc and Nb_{457}-Fc neutralized 100% and 75% of the tested subtype AE viruses with IC_{90} values of <1 nM, respectively (Fig. 3d–f). Particularly striking was Nb457's exceptional potency across almost various subtypes, attaining IC_{90} values below 1 nM (Fig. 3e).

Our findings suggest that Nb_{434}-Fc and Nb_{457}-Fc exhibit more potent and broad neutralization than Ibalizumab. Furthermore, these two nanobodies and Ibalizumab were also tested independently in a collaborative laboratory at Tsinghua University against a panel of 58 HIV-1 pseudoviruses, with average IC_{90} values of 0.1 μg/ml (1.23 nM) and 0.1 μg/ml (1.28 nM), respectively, while Ibalizumab exhibited an average IC_{90} value of 2.49 μg/ml (16.57 nM) (Supplementary Table 3). In this experiment, Ibalizumab neutralized only 60.3% (25/58) of the pseudoviruses with IC_{90} values of less than 50 μg/ml (333.33 nM), while Nb_{434}-Fc and Nb_{457}-Fc neutralized 100% and 96% (56/58) of the tested viruses, respectively (Supplementary Table 3), in agreement with our lab's findings (Fig. 3 and Supplementary Table 2).

Collectively, our findings provide compelling evidence that both Nb_{434}-Fc and Nb_{457}-Fc exhibit superiority over Ibalizumab, showcasing significantly improved average IC_{90} values and broader neutralization breadth.

Structural analysis of Nb457 binding to CD4

Nb_{457}-Fc displays exceptional binding affinity and superior neutralizing potency compared to Nb_{434}-Fc (Fig. 3b and Supplementary Fig. 7a, b), making it the preferred candidate for subsequent in-depth characterization and evaluation. To elucidate the molecular mechanisms underlying the potent neutralization of HIV-1 by Nb457, we determined the crystal structure of the Nb457-D1D2 of CD4 complex at a resolution of 1.81 Å (PDB: 8W90) with a final R_{work} of 0.186 and R_{free} of 0.206. Statistics on diffraction data collection, processing and structural refinement were listed (Supplementary Table 4 and Supplementary Fig. 9). The final model contained three complexes of Nb457-D1D2 of CD4 per asymmetric unit. The buried surface area (BSA) between the Nb457 and CD4 around was approximately 700 $Å^2$ (Fig. 4a, b). The CDR1 of Nb457 was not involved in the recognition of CD4. By contrast, the CDR2 and CDR3 of Nb457 mainly interacted with the side loops (loops 1-3) of D1 and D2, and a total of 18 residues of CD4 constituted the epitope (Fig. 4a–e). Specifically, the CDR2 interacted with specific counterparts on the CD4 and contributed the core interaction interface. The residues W53, Y57 and N59 of CDR2 formed three hydrogen bonds with N32, E92 and P122 of CD4, respectively (Fig. 4d). Notably, D62 of CDR2 established crucial hydrogen bond network with G123, S125 and Q163 of CD4. While, CDR3 provided two hydrogen bonds contribution, forming by S104, Y106 of Nb457 and S79, K1 of CD4 (Fig. 4d, e and Supplementary Fig. 10). Besides the hydrogen bond, a panel of 16 residues further strengthened the Nb457-CD4 binding with extra hydrophobic interactions (Fig. 4c and Supplementary Fig. 10).

To further explore the mechanism by which Nb457 inhibits HIV-1 entry into CD4 cells, we superimposed the CD4-Nb457 complex with the CD4-gp120 complex of HIV-1(PDB: 6L1Y)[22]. Our analysis revealed that the binding site of Nb457 was distinct from that of gp120 (Supplementary Fig. 11a). Specifically, Nb457 binding induced substantial conformational changes in the interface of the D1 domain of CD4. Previous studies have highlighted the critical role of D1 in interacting with a pocket formed by gp120 trimer, particularly implicating residue F43 of D1 in this interaction[23]. Conversely, in our structure, the binding of Nb457 induced the CD4 loop in which F43 is located to bend downward, pulling F43 away from the nexus of gp120 domains (Fig. 4f). To validate these structural perturbations, we performed binding assays employing D1D2 of CD4 and CD4 with gp140 trimers (comprising three subunits of gp120 and the gp41 ectodomain), respectively. Our results showed that Nb457 hindered the binding of D1D2 to gp140 (Fig. 4g). Notably, pre-binding of D1D2 with gp140 did not significantly affect the subsequent binding of Nb457 to CD4 (Fig. 4h). Similar observations were noted regarding the impact of Nb457 on the binding of CD4 protein (Containing D1-D2-D3-D4) to gp140 trimer (Supplementary Fig. 12a, b). Collectively, these findings substantiate that Nb457 disrupts the interaction between CD4 and gp120 by inducing conformational changes in the recognition interface of D1 to gp120.

Furthermore, comparative analysis of the structural complex of Nb457 with that of Ibalizumab (PDB: 3O2D)[24] revealed partial epitope overlap (Supplementary Fig. 11b), as corroborated by FACS analysis (Supplementary Fig. 13a–e). To elucidate the influence of Nb457 binding to CD4 on CD4 binding to MHC-II, we aligned the Nb457-CD4 complex with the CD4-MHC-II complex (PDB: 3T0E)[25], revealing that the Nb457 binding sites are situated on the opposite side of the MHC-II binding sites, exerting a negligible effect on MHC-II binding (Supplementary Fig. 11c). These findings are in

https://doi.org/10.1038/s41467-024-51414-6

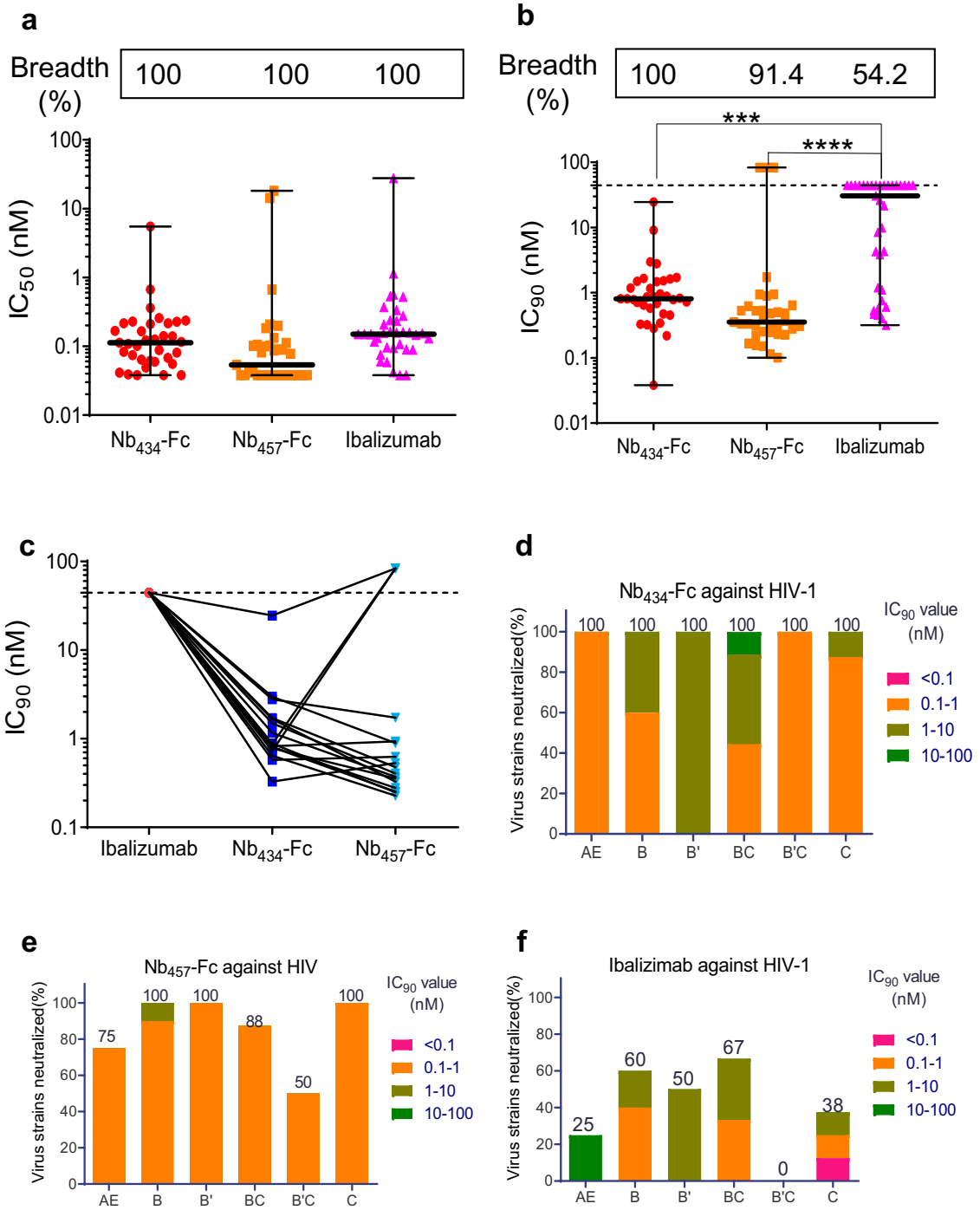

Fig. 3 | Neutralizing HIV-1 pseudoviruses infection by Nbs. a, **b** Graphs depicting the breadth and IC_{50} (**a**) and IC_{90} (**b**) values of Nb_{434}-Fc and Nb_{457}-Fc compared with the broadly neutralizing antibody (bnAb) Ibalizumab with the format of whole IgG against the panel of 35 pseudoviruses of various subtypes ($n = 35$). Equimolar concentration (nM) was used for comparison, considering the differing molecular weights of Ibalizumab and Nbs. Error bars indicate the mean with 95% confidence interval (CI). The "Breadth" in the figure indicates the percentage of pseudoviruses in the tested panel that have been neutralized. At IC_{50}, the breadth represents the percentage of pseudoviruses neutralized at the half-maximal inhibitory concentration, whereas at IC_{90}, it represents the percentage neutralized at the ninetieth percentile inhibitory concentration. One-way two-sided ANOVA with Bonferroni's multiple comparison was used for statistical analysis. ***$P < 0.001$; ****$P < 0.0001$. No statistical differences were observed between Nb_{434}-Fc and Nb_{457}-Fc compared to Ibalizumab ($p = 0.6819$ and $p = 0.998$, respectively) in panel **a**. Significant differences were observed between Nb_{434}-Fc and Nb_{457}-Fc compared to Ibalizumab ($p < 0.0001$ and $p = 0.0002$, respectively) in panel **b**. **c** Graph illustrating the IC_{90} values of Ibalizumab compared with Nb_{434}-Fc and Nb_{457}-Fc against Ibalizumab-resistant viruses. The analysis is based on the results from panel **b**. **d**–**f** Graphs showing the IC_{90} values of Nb434 (**d**), Nb457 (**e**) and Ibalizumab (**f**) in neutralizing various subtypes of HIV-1 pseudoviruses infection, as determined by the neutralization results from panel **b**. The neutralization percentage is indicated in the figure. Source data are provided as a Source Data file.

https://doi.org/10.1038/s41467-024-51414-6

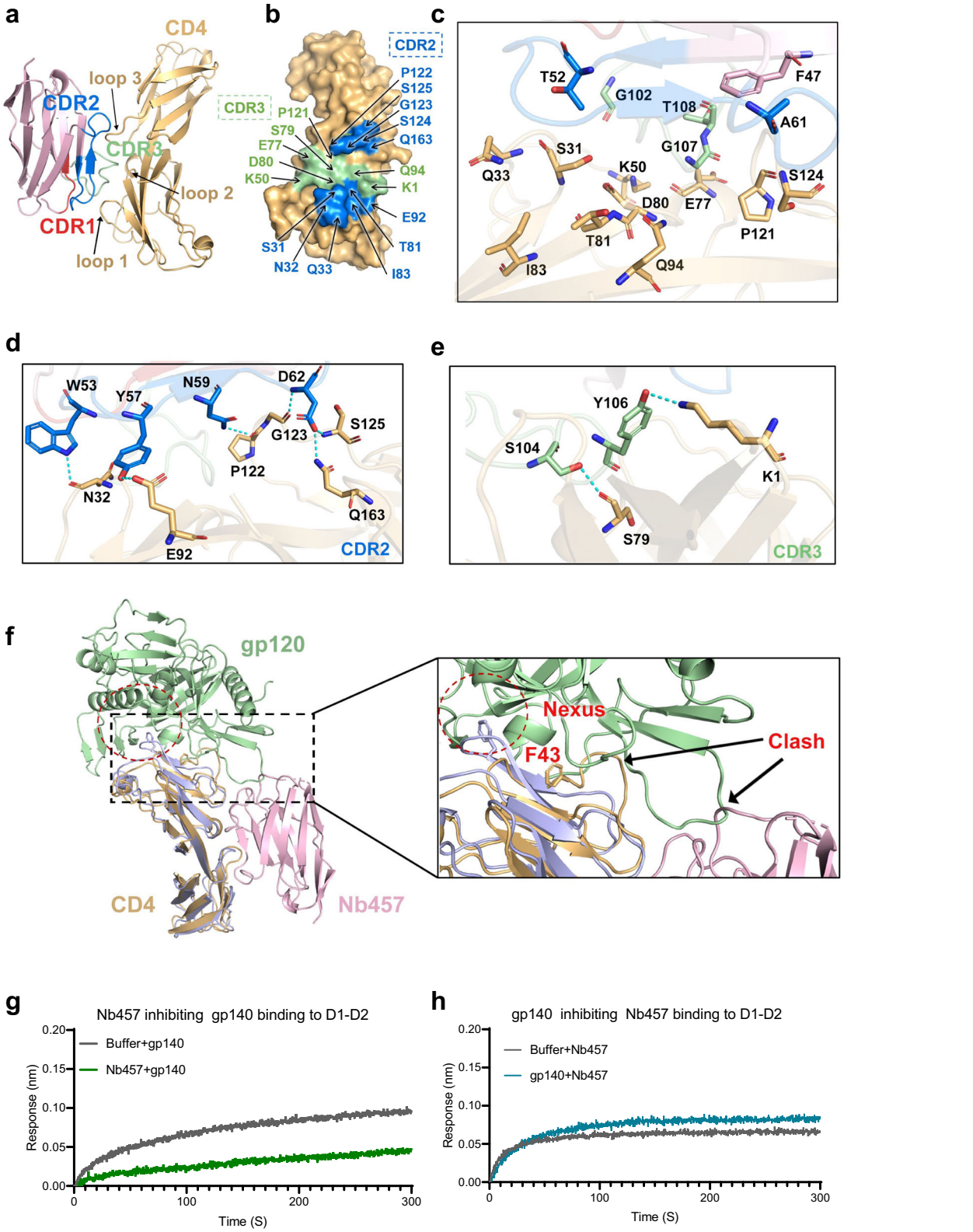

agreement with our experimental data, which demonstrated that Nb457 binding had no discernible impact on CD4 binding to MHC-II on Daudi cells (Supplementary Fig. 14a–c). Taken together, our results suggest that the predominant binding sites of Nb457 reside at the junction of D1-D2, inducing conformational changes in D1 that impede gp120 binding and potentially contribute to its potent neutralization of HIV-1.

Nb457-based trimeric nanobodies exhibited enhanced potency against HIV-1 virus

In order to mitigate potential side-effects associated with the Fc fusion tag and to extend the in vivo half-life of Nb_{457}, we employed a trimeric VHH format for Nb_{457}, termed Nb_{457}-Nb_{HSA}-Nb_{457} (~40 kDa) (Fig. 5a), following a strategy developed in our laboratory[15]. This construct targets CD4 protein through Nb457, while simultaneously harnessing the

Fig. 4 | Structural characterization of the Nb457 and CD4 complex. a Overall configuration of the intricate assembly formed by Nb457 and the D1-D2 domains of CD4. Complementarity Determining Regions (CDRs) of Nb457 are color-coded: CDR1 (red), CDR2 (blue), CDR3 (green), while the D1-D2 domains of CD4 are depicted in orange, utilizing a schematic cartoon representation. **b** The epitope recognized by Nb457 shown in surface representation. The regions interacted by CDR2 and CDR3 are colored blue and green, respectively. **c** Hydrophobic network between Nb457 and the D1-D2 domains of CD4, elucidated through a representation of amino acid residues in stick conformation. **d, e** Elucidation of the interface involving Nb437 and the D1-D2 domains of CD4. CDR regions are differentially color-highlighted in red, blue, and green. Noteworthy interactions within CDR2 (**d**) and CDR3 (**e**) are accentuated, with hydrogen bonding interactions depicted as cyan dashed lines. **f** Comparative overlay of the CD4-gp120 (PDB: 6L1Y) (light blue and green) complex and the CD4-Nb457 (orange and pink) complex. Discernible conformational variations in CD4 upon association with Nb457 are juxtaposed against the CD4 arrangement within the gp120-CD4 interface. The inset rectangle magnifies the altered interaction interface. **g** Binding kinetics of gp140 to D1-D2 protein in the presence of Nb457 were assessed by BLI. D1-D2 fragments of the CD4 protein were immobilized on biosensors. A solution containing 300 nM Nb457 or buffer only as a control was loaded onto the biosensors for 300 s to achieve saturation binding. After a 60 s baseline equilibration with binding buffer, 300 nM gp140 was introduced to measure the association curve. The gp140 utilized in this assay consisted of native-like BG505 SOSIP gp140, comprising three subunits of gp120 and gp41 ectodomain. **h** Binding kinetics of Nb457 to D1-D2 protein in the presence of gp140 were determined by BLI. D1-D2 fragments of the CD4 protein were immobilized on biosensors. A solution containing gp140 or buffer only as a control was loaded onto the biosensors for 300 s to achieve saturation binding. Following a 60 s baseline equilibration with binding buffer, 300 nM Nb457 was introduced to measure the association curve. Source data are provided as a Source Data file.

binding capacity of Nb_{HSA} towards both human serum albumin (HSA) and murine serum albumin (MSA) proteins, thus offering the potential for improved in vivo stability[14]. As expected, the Nb_{457}-Nb_{HSA}-Nb_{457} construct exhibited impressive binding affinities with both CD4 protein and HSA protein, yielding measured KD values of 4.2 nM and 29.4 nM, respectively (Supplementary Fig. 15a–c).

To comprehensively assess the breadth and potency of Nb_{457}-Nb_{HSA}-Nb_{457} against HIV-1 variants, we conducted neutralization analysis utilizing a global panel of 12 well-characterized HIV-1 pseudoviruses, selected from a pool of 219 Env-pseudotyped viruses representing prevalent global variants[26]. Our findings reveal that Nb457 successfully neutralized 11 out of 12 HIV-1 pseudoviruses in this panel. Notably, Nb_{457}-Nb_{HSA}-Nb_{457} exhibited potent neutralizing activity, with an average IC_{90} value of 0.06 μg/ml (1.5 nM), surpassing that of Nb_{457}-Fc (0.28 μg/ml, 3.55 nM) and Ibalizumab (0.91 μg/ml, 6.08 nM) (Supplementary Fig. 16a, b).

For identification of resistant viruses, we assembled a panel of broad-resistant HIV-1 pseudoviruses for further evaluation. This panel comprised 12 pseudoviruses defined as strains resistant to at least 10 of the 16 CD4 binding site broadly neutralizing antibodies (bnAbs), with an IC_{50} exceeding 50 μg/ml[27]. Surprisingly, both Nb_{457}-Fc and Nb_{457}-Nb_{HSA}-Nb_{457} effectively neutralized all tested broad-resistant viruses (Supplementary Fig. 17a, b), indicating a low likelihood of resistance development against Nb457.

To further evaluate the neutralization potential of Nb457, live HIV-1 virus was employed. Remarkably, Nb_{457}-Nb_{HSA}-Nb_{457} demonstrated significantly enhanced neutralization activity against live HIV-1 infection when compared to the Nb_{457}-Fc and Ibalizumab. Notably, Nb_{457}-Nb_{HSA}-Nb_{457} neutralized all five representative strains of tested HIV−1 live virus, including tier 1 and tier 2 variants, with an average IC_{50} value of 0.09 μg/ml (2.37 nM) and an average IC_{90} value of 0.36 μg/ml (9.02 nM) (Fig. 5b–g). In contrast, the Nb_{457}-Fc neutralized the same set of HIV−1 live virus strains with an average IC_{50} value of 0.07 μg/ml (0.83 nM) and exhibited IC_{90} values ranging from 0.07 μg/ml to 0.33 μg/ml (0.77–4.03 nM) only for four out of five strains (Fig. 5b–g). As for Ibalizumab, it neutralized all tested HIV−1 live virus strains with an average IC_{50} value of 0.5 μg/ml (3.31 nM) and IC_{90} values ranging from 0.15 μg/ml to 2.88 μg/ml (1.01–19.2 nM) only for two out of five strains (Fig. 5b–g). In aggregate, Nb_{457}-Nb_{HSA}-Nb_{457}, Nb_{457}-Fc and Ibalizumab achieved 100%, 80% and 40% inhibition, respectively, against live HIV−1 infection at the 90% inhibition level.

Notably, Ibalizumab exhibited neutralization curves that plateaued below complete inhibition for all five strains of the tested live HIV−1 virus, a trend that aligns with previous reports[24] (Fig. 5b–g). Similarly, the Nb_{457}-Fc construct displayed inhibition curves with maximum percent inhibition (MPI) below 100%, specifically against the live HIV-1_{BAL} and HIV-1_{CH058} strains (Fig. 5b–g). Such strains with MPI values below 100% may harbor the potential to elude the inhibitory effects of Ibalizumab or Nb_{457}-Fc. In contrast, Nb_{457}-Nb_{HSA}-Nb_{457} achieved the complete neutralization of all five strains of the tested live HIV-1 virus, as evidenced by an MPI value of 100% (Fig. 5b–g). This finding underscores a significantly diminished likelihood of viral escape when employing Nb457-based trimeric nanobodies. In summary, the unique structural arrangement of Nb_{457}-Nb_{HSA}-Nb_{457} demonstrated superior neutralization efficacy across the entire spectrum of tested HIV-1 live virus strains, with an MPI value attaining the optimal threshold of 100%.

Molecular dynamics simulation indicated structural basis for complete inhibition of HIV-1_{CH058} by Nb457-based trimeric nanobodies

To elucidate the phenomenon wherein Nb_{457}-Fc exhibited sub-100% inhibition of live HIV-1_{CH058} infection, akin to Ibalizumab, while Nb_{457}-Nb_{HSA}-Nb_{457} demonstrated complete 100% inhibition against HIV-1_{CH058} infection (Fig. 5c), we established three distinct systems: CD4 and gp120 (derived from the HIV-1_{CH058} sequence) (Supplementary Fig. 18a), CD4, gp120 (HIV-1_{CH058} sequence), and Nb_{457}-Fc (Supplementary Fig. 18b), and CD4, gp120 (HIV-1_{CH058} sequence), and Nb_{457}-Nb_{HSA}-Nb_{457} (Supplementary Fig. 18c). Each of these systems underwent a rigorous 500 ns molecular dynamics (MD) simulation, with the final 400 ns chosen for subsequent analysis (Supplementary Data 1–6). Our primary focus was centered on evaluating the CD4 and gp120 interaction, examining two critical aspects: the count of main-chain hydrogen bonds, pivotal in their binding (Supplementary Fig. 18d), and the Root Mean Square Fluctuation (RMSF) values specifically concerning the D1-D2 domain of CD4 (Supplementary Fig. 18e).

We scrutinized the temporal dynamics of main-chain hydrogen bonds within these three systems. When the tally of hydrogen bonds reached or surpassed 1, it signified an interaction between CD4 and gp120, prompting us to record the conformations at these junctures. Subsequently, we generated bar chart to visually represent this data (Supplementary Fig. 18d). Additionally, we computed the mean number of main-chain hydrogen bonds for each system. The system devoid of nanobodies exhibited a mean value of 0.91, while the systems incorporating Nb_{457}-Fc and Nb_{457}-Nb_{HSA}-Nb_{457} displayed mean values of 0.21 and 0.13, respectively (Supplementary Fig. 18d). This suggests that Nb_{457}-Fc and, particularly, Nb_{457}-Nb_{HSA}-Nb_{457}, may reduce the number of main-chain hydrogen bonds in the CD4 and gp120 interaction, with Nb_{457}-Nb_{HSA}-Nb_{457} having a more pronounced effect.

Through cluster analysis, we identified the most probable conformations for each system and pinpointed their main-chain hydrogen bonds. In the absence of antibodies, the system featured two primary main-chain hydrogen bonds, specifically between K46 of CD4 and G330 of gp120, and between L44 of CD4 and D332 of gp120 (Supplementary Fig. 18a). In contrast, systems containing Nb_{457}-Fc displayed a single main-chain hydrogen bond, linking K46 of CD4 with G331 of gp120 (Supplementary Fig. 18b). Similarly, for systems encompassing Nb_{457}-Nb_{HSA}-Nb_{457}, we observed a single main-chain hydrogen bond,

https://doi.org/10.1038/s41467-024-51414-6

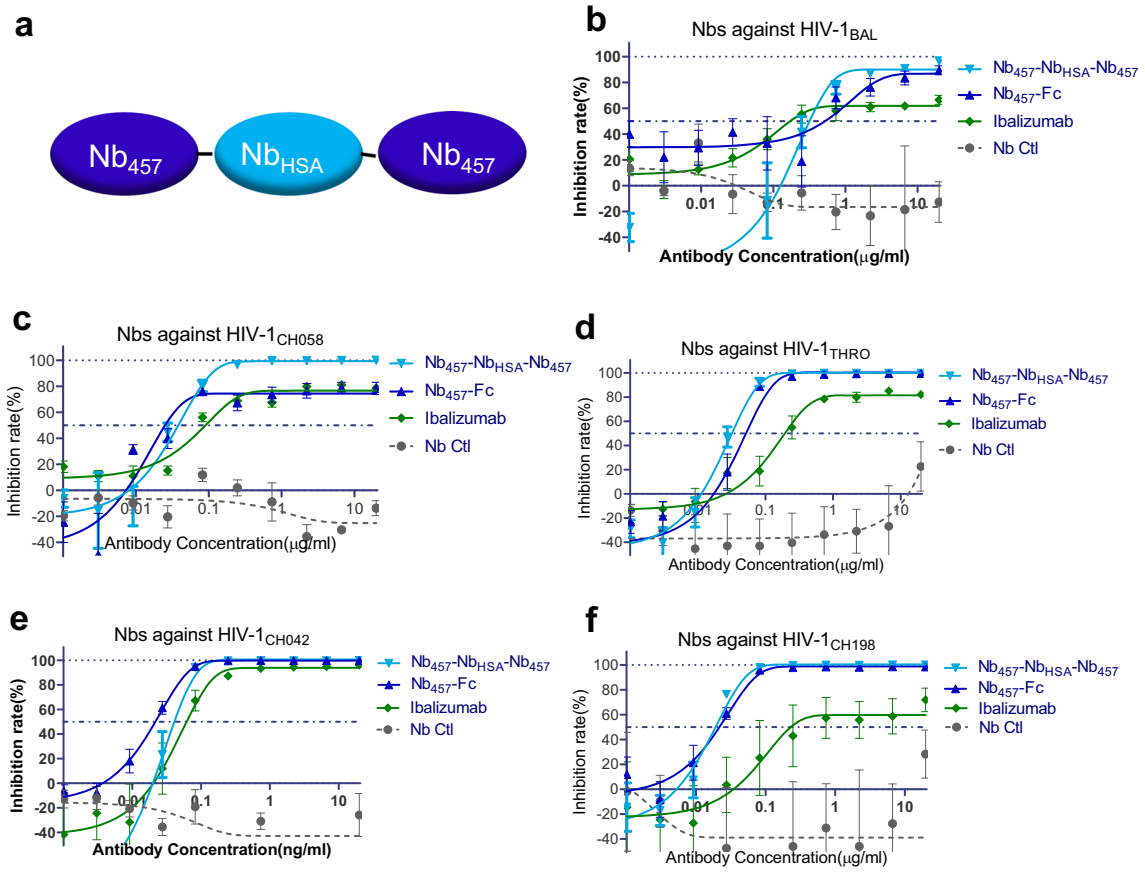

g

Virus Name	Subtype	Year of isolation	Tier	μg/ml	Nb_{457}-Nb_{HSA}-Nb_{457}	Nb_{457}-Fc	Ibalizumab	Nb Ctl
BAL	B	1985	1b	IC_{50}	0.3585	0.1798	0.6730	>20
				IC_{80}	0.6969	17.5780	>20	>20
				IC_{90}	1.0280	>20	>20	>20
				IC_{100}	20.0000	>20	>20	>20
CH058	B	2006	2	IC_{50}	0.0341	0.0688	0.1449	>20
				IC_{80}	0.0624	0.3919	2.5730	>20
				IC_{90}	0.0889	1.0840	>20	>20
				IC_{100}	0.7407	>20	>20	>20
THRO	B	2000	2	IC_{50}	0.0277	0.0440	0.2660	>20
				IC_{80}	0.0322	0.0643	1.1970	>20
				IC_{90}	0.0342	0.0803	2.8840	>20
				IC_{100}	0.2469	0.7407	>20	>20
CH042	C	2007	2	IC_{50}	0.0340	0.0214	0.0640	>20
				IC_{80}	0.0434	0.0418	0.1099	>20
				IC_{90}	0.0437	0.0619	0.1508	>20
				IC_{100}	0.2469	0.2469	>20	>20
CH198	C	2007	2	IC_{50}	0.0195	0.0207	1.3330	>20
				IC_{80}	0.0291	0.0429	>20	>20
				IC_{90}	0.0368	0.0658	>20	>20
				IC_{100}	0.2469	0.2469	>20	>20

Fig. 5 | Neutralizing efficacy of Nb457 against live HIV-1 virus infection. **a** Illustration of the schematic structure of Nb_{457}-Nb_{HSA}-Nb_{457}, wherein the trimeric Nbs are interconnected by (G4S)3 linker. **b**–**f** Assessment of the neutralizing effects of Nb_{457}-Nb_{HSA}-Nb_{457} (cyan line), Nb_{457}-Fc (blue line) and Ibalizumab (green line) against five distinct live HIV-1 strains: HIV-1_{BAL} (subtype B) (**b**), HIV-1_{CH058} (subtype B) (**c**), HIV-1_{THRO} (subtype B) (**d**), HIV-1_{CH042} (subtype C) (**e**), and HIV-1_{CH198} (subtype C) (**f**). The negative control nanobody, Nb Ctl (gray dashed line), was employed. Data are presented as the mean ± standard error of the mean (SEM). **g** Compilation of IC_{50}, IC_{80}, IC_{90} and IC_{100} values alongside the corresponding data from the neutralization assay performed on live HIV-1 viruses, as detailed in panels **b**–**f**. Source data are provided as a Source Data file.

precisely between Q33 of CD4 and G415 of gp120 (Supplementary Fig. 18c).

Investigation of the impact of anti-CD4 Nbs on CD4$^+$ T cells

To assess the impact of Nb457 on CD4 binding with MHC II, we initially incubated CD4-rFc protein with Nbs and subsequently evaluated its binding with MHC-II on Daudi cells. The CD4-rFc protein exhibited a dose-dependent binding with Daudi cells, as determined by flow cytometry (Supplementary Fig. 14b). Control Nb, Nb_{457}-Fc, Nb_{457}-Nb_{HSA}-Nb_{457}, and Ibalizumab at concentrations ranging from 0.03 to 2 μg/ml revealed no discernible impact on CD4 binding with MHC-II on Daudi cells (Supplementary Fig. 14c), which agreed with the structural analysis (Supplementary Fig. 11c).

To evaluate the effects of Nb457 on T cell proliferation, we incubated PBMCs from healthy donors, with or without PHA stimulation, along with Nb457 and control Nbs for 4 days. Intracellular expression of the cell proliferation marker Ki67 was measured by flow cytometry. Compared to unstimulated conditions, Ki67 expression was significantly increased with PHA stimulation (Supplementary Figs. 19a, 20a). Notably, the results demonstrated that treatments with control Nb, Nb_{457}-Fc, Nb_{457}-Nb_{HSA}-Nb_{457}, and Ibalizumab did not show any significant difference in Ki67 expression in CD4$^+$ T cells under both PHA stimulation and unstimulated conditions (Supplementary Figs. 19a, 20a). These findings suggest that Nb_{457}-Fc and Nb_{457}-Nb_{HSA}-Nb_{457} do not exhibit any discernible impact on CD4$^+$ T cell proliferation.

As a quantitative measure of T cell activation, we conducted an evaluation of an early activation marker (CD69) and the interleukin (IL)-2 receptor α chain (CD25) on CD4$^+$ T cells (Supplementary Figs. 19a, 20b, c). Across samples from the same donor and stimulation, we observed highly similar activation profiles for all Nb treatments. The percentage of CD4$^+$CD25$^+$ cells steadily increased over time under PHA-stimulated condition, with the percentage of positive cells consistently remaining high at all analytic points (Supplementary Fig. 19a, 20b, c). Importantly, irrespective of inter-donor variations, treatments with Nb457, Ibalizumab or control Nb did not result in significant differences in the percentage of CD4$^+$CD25$^+$ or CD4$^+$CD69$^+$ cells under both conditions of PHA stimulation and unstimulated conditions (Supplementary Figs. 19a, 20b, c).

Subsequently, we conducted an analysis of cytokine expression in CD4$^+$ T cells through intracellular cytokine staining. Samples were treated with different antibodies with or without PHA stimulation. Notably, samples treated with control Nb, Nb_{457}-Fc, Nb_{457}-Nb_{HSA}-Nb_{457} and Ibalizumab exhibited remarkably similar percentages of cytokine expression, including IL-2, IFN-γ and tumor necrosis factor (TNF-α) under either PHA stimulation or unstimulated conditions (Supplementary Figs. 19b, 20d–f).

Taken together, our findings demonstrated that exposure to Nb_{457}-Fc or Nb_{457}-Nb_{HSA}-Nb_{457} did not exert any significant impact on MHC-II binding with CD4, proliferation, activation, or cytokine production of CD4$^+$ T cells. These results highlight the safety and potential therapeutic value of Nb_{457}-Fc or Nb_{457}-Nb_{HSA}-Nb_{457}.

Therapeutic efficacy of Nb457 treating HIV-1-infected humanized NDG-HuPBL mice

To assess the in vivo efficacy of Nb457 in treating HIV-1 infection, a humanized mouse model (NDG-HuPBL) with HIV-1 infection was established following our established protocols[8] (Fig. 6a). These mice were challenged with 10 ng of P24 HIV-1_{CH058}, originating from a transmitted/founder virus, known to be a tier 2 virus, and exhibiting resistance to most antibody neutralization[28]. Notably, neutralization assays revealed potent inhibition of HIV-1_{CH058} by Nb_{457}-Fc, Nb_{457}-Nb_{HSA}-Nb_{457} and Ibalizumab. However, both Nb_{457}-Fc and Ibalizumab failed to achieve complete neutralization even at the highest doses. In contrast, Nb_{457}-Nb_{HSA}-Nb_{457} demonstrated remarkable efficacy, achieving 100% inhibition at 0.2469 μg/ml (Fig. 5c, g).

Given that intraperitoneal (*i.p.*) administration of Nb457 resulted in a rapid attainment of peak serum concentration (C_{max}) but with a short half-life, while subcutaneous (s.c.) administration necessitated a longer time to reach Cmax but conferred a longer half-life (Supplementary Fig. 21a–c), we adopted a combination approach for evaluating Nb457 in vivo. As such, to evaluate the therapeutic effects, we administered 400 μg/mouse of each antibody via *i.p.* plus *s.c.* routes to HIV-1 infected NDG-HuPBL mice ($n = 4$) at 1 day, 3 days, 5 days and 7 days post-infection (Fig. 6a). The viral load in blood was monitored on a weekly basis for four weeks post-infection and revealed a progressive increase in the control group, while the treatment groups displayed significantly lower viral loads compared to the Nb Ctl group. Notably, Ibalizumab and Nb_{457}-Nb_{HSA}-Nb_{457} groups exhibited substantial reductions in viral loads by 2 to 5 logs at 3 and 4 weeks post-infection (Fig. 6b). To further validate the viral load, we isolated spleenocytes from sacrificed mice and cultured them ex vivo for two days, followed by viral RNA quantification in cell supernatants. Viral RNA levels in cell supernatants from Nb457 or Ibalizumab-treated mice were significantly lower compared to the control Nb treatment (Fig. 6c). Notably, 2/4 cell supernatants from the Nb_{457}-Nb_{HSA}-Nb_{457}-treated group exhibited undetectable viral RNA, in agreement with the viral RNA levels in the blood (Fig. 6b, c). Immunofluorescence staining of P24 in the spleen corroborated these findings, showing reduced P24$^+$ positive cells in Nb457-Fc or Ibalizumab-treated groups, and only a scattered and limited presence of P24$^+$ positive cells in mice treated with Nb_{457}-Nb_{HSA}-Nb_{457} (Fig. 6d).

In conclusion, our study demonstrated the robust inhibitory effects of Nb_{457}-Nb_{HSA}-Nb_{457}, along with Nb_{457}-Fc and Ibalizumab, on HIV-1 replication in vivo. Notably, Nb_{457}-Nb_{HSA}-Nb_{457} exhibited high efficacy, as evidenced by the VOA assay and immunostaining of the spleen.

Discussion

The development of effective therapies for HIV-1 infection remains a formidable challenge. Ibalizumab, the sole antibody drug with specific binding to CD4, has demonstrated therapeutic efficacy against multidrug-resistant HIV-1 isolates[6,7], highlighting CD4 as a promising target for HIV-1 drug development. However, the limited breadth, potency and MPI less than 100% of Ibalizumab pose challenges for long-term treatment and raise concerns about the potential to the development of antibody resistance. Clearly, more potent and broadly effective antibodies are needed. This can be achieved either by isolating antibodies with exceptional neutralizing activity using strategies or engineering existing antibodies into bi- or tri-specific combinations. Previously, we reported the development of the bispecific antibody BiIA-SG, which combines two single-chain variable fragment (scFv) binding domains of Ibalizumab and the broadly neutralizing antibody PGT-128, targeting HIV gp120[8,9]. BiIA-SG significantly improved the breadth and potency of Ibalizumab and provided functional cure in humanized mouse and macaque models[8,9], further highlighting the potential of CD4 antibodies in the development of HIV-1 therapeutics.

In recent years, nanobodies have emerged as a promising alternative to traditional antibodies for drug development owing to their unique advantages. While several anti-CD4 nanobodies have been developed for tracing CD4 cells in vivo[21], their potential as therapeutics for neutralization against HIV-1 infection has yet to be explored. To address this gap, we isolated a panel of anti-CD4 nanobodies from an alpaca immunized with human CD4, and found that Nb457 in particular has significant potential as a therapy for HIV-1 infection. Our extensive neutralization testing, encompassing 93 different HIV-1 isolates, which included 35 isolates assessed at Nanjing University and additional 58 isolates evaluated at Tsinghua University, revealed that

https://doi.org/10.1038/s41467-024-51414-6

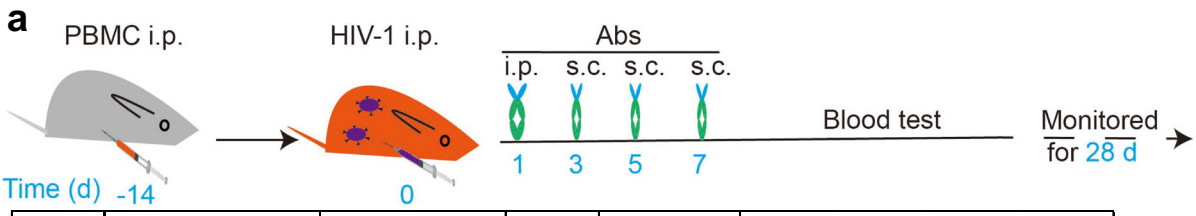

Group	Name	Reagent	Numbers (n)	HIV-1_{CH058} Challenge i.p.	Antibody Infusion			
				0d	1d (i.p.)	3d (s.c.)	5d (s.c.)	7d (s.c.)
Group 1	Nb_{457}-Fc	Nb_{457}-Fc4	4	√	√	√	√	√
Group 2	Nb_{457}-Nb_{HSA}-Nb_{457}	Nb_{457}-Nb_{HSA}-Nb_{457}	4	√	√	√	√	√
Group 3	Ibalizumab	Ibalizumab	4	√	√	√	√	√
Group 4	Nb Ctl	SNB02	4	√	√	√	√	√
Group 5	No HIV-1	\	4	\	\	\	\	\

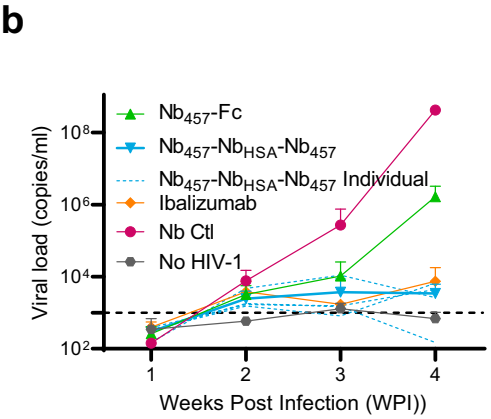

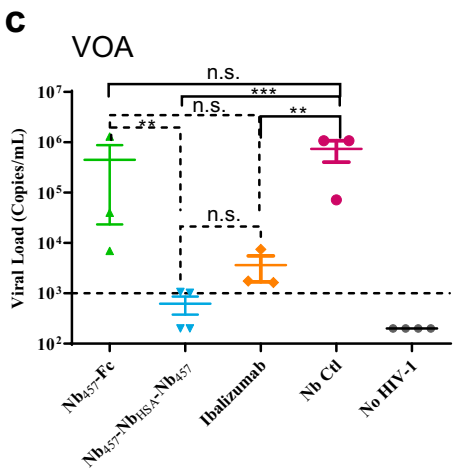

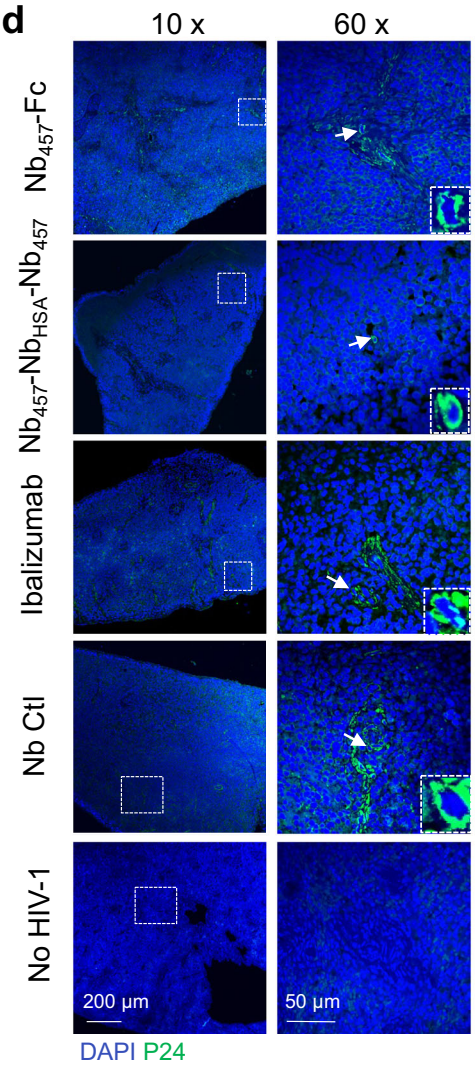

Nb457 had both significantly superior neutralizing potencies and a much broader spectrum of activity against HIV-1 than Ibalizumab, which was more potent than those of the broadly neutralizing monoclonal antibodies PG9 and VRC01[7]. Specifically, the IC_{90} of Nb457 was 0.6 μg/ml, with a neutralization of 91.4% of the isolates, indicating that the potency and broad activity of Nb457 is nearly 5 times and 90% higher than Ibalizumab, respectively. Notably, among the reported anti-HIV antibodies with ultrapotent neutralization capacity[29–32], Nb457 stands out with one of the lowest IC_{90} values, underscoring its exceptional potency. Furthermore, its broad-spectrum activity against over 90% of the isolates suggests that HIV-1 is less likely to develop resistance to Nb457. Thus, Nb457, as the alpaca-derived neutralizing nanobody binding to CD4, represents a potent and highly broadly neutralizing nanobody against diverse HIV-1 genotypes.

Fig. 6 | Therapeutic efficacy of Nb457s in HIV-1-infected NDG-HuPBL mice. **a** Experimental timeline outlining the immunotherapeutic intervention using Nb457 and Ibalizumab in HIV-1_{CH058}–challenged humanized mice. Intraperitoneal (i.p.) injections were administered at 1 day post-infection (dpi), followed by subcutaneous (s.c.) administrations at 3 dpi, 5 dpi, and 7 dpi after HIV-1_{CH058} challenge. Each treatment group received four administrations, including Nb_{457}-Fc, Nb_{457}-Nb_{HSA}-Nb_{457}, Ibalizumab, and a negative control Nb (Nb Ctl, SNB02, one of our published nanobodies specific for envelope protein of SFTSV). The dosage of Nbs or antibodies was 400 μg (~20 mg/kg). The initial HIV-1 inoculum was 10 ng P24. Mice were monitored for four weeks post HIV-1 challenge. A summary of the treatment groups ($n = 4$ mice, female) with distinct interventions is presented in the lower table. **b** Quantification of plasma viral loads in five groups of NDG-HuPBL mice, color-coded and labeled as in the table in (**a**), assessed through qRT-PCR. Nb_{457}-Fc (green line), Nb_{457}-Nb_{HSA}-Nb_{457} (cyan line), Ibalizumab (orange line), and Nb Ctl (pink line), No HIV-1 (gray line). Each line represents average data from one group of mice ($n = 4$ in each group). Data from an individual mouse in the Nb_{457}-Nb_{HSA}-Nb_{457} group is represented by a cyan dashed line. Data are presented as SEM. **c** Viral outgrowth assay (VOA) results of splenocytes from the aforementioned HIV-1-infected NDG-HuPBL mice ($n = 4$ in each group), indicating viral load in copies per milliliter culture supernatant. Data are presented as mean ± SEM. Two-sided Mann–Whitney test was applied to compare the treatment group with the Nb control group. Significance levels: ns, not significant; $^{*}p < 0.05$, $^{**}p < 0.01$, $^{***}p < 0.001$. **d** Immunofluorescence staining of spleen sections using antibodies specific to HIV-1 nucleocapsid protein (P24) in green, and DAPI (4′,6-diamidino-2-phenylindole) for nuclei in blue. Representative spleen sections were visualized under ×10 or ×60 objective, with indicated scale bars (200 μm or 50 μm), respectively. Source data are provided as a Source Data file.

An intriguing finding was observed when comparing trimeric Nb457 (Nb_{457}-Nb_{HSA}-Nb_{457}) with Ibalizumab and Nb_{457}-Fc. Ibalizumab demonstrated inhibition curves with MPI values consistently below 100% across all five live HIV-1 strains tested, while Nb_{457}-Fc exhibited similar MPI values but only against the HIV-1_{BAL} and HIV-1_{CH058} strains. In contrast, our engineered Nb457-based trimeric nanobodies, Nb_{457}-Nb_{HSA}-Nb_{457}, displayed complete neutralization of various HIV-1 live strains, achieving an MPI value of 100%. This exceptional outcome suggests a significantly reduced likelihood of viral escape when utilizing Nb_{457}-Nb_{HSA}-Nb_{457} nanobody.

Structural analysis of Nb457 binding to CD4 offers crucial insights into its mechanism of action against HIV-1 infection. The crystal structure determination of the Nb457-D1D2 of CD4 complex reveals intricate interactions, highlighting the involvement of CDR2 and CDR3 regions in forming a binding epitope comprising 18 CD4 residues. Notably, our comparison with Ibalizumab's structural complex demonstrates partial epitope overlap, supported by FACS analysis. Furthermore, upon superimposing the CD4-Nb457 complex with the CD4-gp120 complex (PDB: 6L1Y), substantial conformational changes induced by Nb457 binding in the CD4 D1 domain were observed, effectively impeding gp120 binding to CD4 cells. Importantly, the epitope of Nb457 was found to be situated on the opposite side of MHC-II binding sites, ensuring minimal interference with MHC-II binding. Our experimental results further confirmed the favorable safety profile of Nb457, as exposure to Nb457 did not disrupt MHC-II binding and the proliferation, activation, or cytokine production of $CD4^{+}$ T cells.

Additionally, the development of Nb_{457}-based trimeric nanobodies, exemplified by Nb_{457}-Nb_{HSA}-Nb_{457}, significantly enhances neutralization potency against a spectrum of HIV-1 live virus strains, achieving complete inhibition with an MPI value of 100%. MD simulations indicated distinct conformational changes induced by Nb_{457}-Nb_{HSA}-Nb_{457} on the interface of the CD4 D1 domain compared to Nb_{457}-Fc. Notably, Nb_{457}-Nb_{HSA}-Nb_{457} binding exerts a more pronounced influence on the main-chain hydrogen bonds between CD4 and gp120 of the HIV-1_{CH058} strain. This interaction likely disrupts the stability of the CD4-gp120 complex, a critical determinant for viral entry. These findings suggest the potential of Nb_{457}-Nb_{HSA}-Nb_{457} to interfere with the CD4-gp120 interaction, thereby enhancing its antiviral efficacy.

In vivo studies conducted in humanized mice have demonstrated the therapeutic efficacy of Nb457 against HIV-1 infection, even when administered subcutaneously. Notably, the application of trimeric nanobodies has shown superior efficacy, further accentuating the potential of these nanobodies as promising therapeutics. Particularly, in the Nb_{457}-Nb_{HSA}-Nb_{457} trimeric nanobodies group, some mice achieved an almost undetectable viral load, as assessed through Q-PCR, VOA, and immunofluorescence staining. These results underscore the efficacy of Nb457 as an effective inhibitor of HIV-1 infection in vivo, with Nb_{457}-Nb_{HSA}-Nb_{457} trimeric nanobodies demonstrating significantly enhanced therapeutic efficacy for the treatment of HIV-1 infection in vivo. These findings underscore the potential of Nb457 as a promising candidate, offering high efficacy in targeting a diverse range of clinical HIV-1 variants, including drug-resistant strains.

The unique properties of nanobodies, including their small size, high thermal stability, and specificity, make them well-suited for a range of biomedical applications, offering a promising avenue for the development of innovative HIV-1 therapeutics. For instance, CD4 nanobodies hold promise for gene therapy applications, enabling in vivo delivery of the CD4 nanobody gene. Additionally, the VHH component of Nb457 nanobody exhibits versatile utility, exemplified by its potential for integration into diverse applications, including the construction of antibody–drug conjugates (ADCs) or its employment in CD4 CAR-T therapy to selectively target CD4+ cells, encompassing CD4 T cells. In addition, the small molecular mass of nanobody makes higher molar production of nanobody per culture unit and the simpler structure allows the production in yeast or bacterial system feasible, which will significantly reduce the cost to the end users, a critical restricting factor for broader application of the antibody-based HIV-1 therapy.

Further characterization of the resistant profile for Nb457 is warranted. Although only one HIV-1 pseudovirus (246_F3_C10_2) exhibited resistance to Nb457 among the 117 tested viruses, encompassing a panels of 35 pseudoviruses in our lab, a panels of 58 pseudoviruses in a collaborative lab at Tsinghua University, a global panel of 12 pseudoviruses[26] and a broad-resistant panel of 12 pseudoviruses[27], indicating a relatively low likelihood of resistance development against Nb457, rigorous characterization and monitoring of resistance profiles for Nb457 during clinical trials are imperative. It is noteworthy that Nb457 demonstrated neutralization efficacy against all viruses within the broad-resistant panel of 12 HIV-1 pseudoviruses, suggesting a distinct resistance profile compared to anti-CD4 binding site antibodies. Further investigation is warranted to explore the potential of anti-CD4 antibodies to complement the efficacy of anti-HIV antibodies in HIV-1 therapy. Despite the successful humanization of Nb457 with no observed impact on its activity, caution must be exercised regarding its immunogenicity in clinical applications. Particular attention should be paid to the risk of anti-Nb457 antibody development, emphasizing the need for careful monitoring and evaluation during clinical trials.

In conclusion, our study represents a significant advancement in the development of ultra-potent anti-CD4 nanobodies as promising therapeutics against HIV-1 infection. The distinct properties exhibited by Nb457, including its non-interference with MHC-II binding and T cell function, alongside its exceptional efficacy against diverse HIV-1 strains, position it as a compelling candidate for further research and therapeutic applications. Importantly, Nb_{457}-Nb_{HSA}-Nb_{457} demonstrated robust protection in some HIV-infected humanized mice, attaining an MPI of 100%, further underscoring its potential as a highly effective candidate for targeting a wide array of clinical HIV-1 variants, including drug-resistant strains.

Methods

Alpaca immunization

The Alpaca immunization procedure was conducted with some adjustments based on our previously published method[33]. Briefly, a female alpaca (Abrev, Ltd., Nanjing, China) aged 2 to 4 years was administered with an initial immunization comprising 250 μg of CD4-rFc protein emulsified with 250 μl of Freund's complete adjuvant (Cat#: F5881-10ML, Sigma). Subsequently, three additional boosts were administered at weeks 2, 4, and 6, each consisting of 250 μg of CD4-rFc protein diluted in 250 μl of Freund's incomplete adjuvant (Cat#: F5506-10ML, Sigma). Blood samples were collected for anti-serum characterization with CD4-His one week following both the 3rd and 4th immunizations. Furthermore, 100 ml of blood was collected one week after the 4th immunization for anti-serum characterization and to develop a phage library displaying the VHH antibody.

SDS-PAGE and Western blotting

Recombinant proteins, engineered with either a rabbit Fc (rFc) tag or His-tag at the C-terminus, were transiently expressed in FreeStyleTM 293-F cells (Cat#: R79007, Thermo Scientific) and subsequently purified from the cell culture supernatant. Commercial Protein A Sepharose (Cat#: 20334, Thermo Scientific) or Ni-NTA (Cat#: R901100, Thermo Scientific) columns were employed for purification, depending on the protein variant. Post-purification, proteins or antibodies were resolved using electrophoresis on a 7.5–12% polyacrylamide gel. Electrophoresis was conducted under reducing and nonreducing conditions to discern the absence and presence of β-mercaptoethanol in the gel-loading buffer, respectively. Protein bands were visualized through either Coomassie blue staining or were transferred onto a PVDF membrane for immunoblotting. After membrane blocking, incubation ensued with the respective antibodies or plasma, either at 4 °C overnight or at 37 °C for 60 min. Subsequently, a secondary antibody, specifically anti-rabbit IgG or anti-human IgG, conjugated with an IRDye 800CW (Cat#: 926-32232, Rockland), was utilized. Protein bands were imaged and analyzed using the Odyssey Image System (Li-COR).

ELISA for characterizing anti-sera and antibody

Antibody characterization and the determination of anti-sera titers were conducted using a modified ELISA protocol, previously established in our laboratory[34]. High protein-binding ELISA plates (Cat#: 9018, Corning) were coated with protein at a concentration of 0.5 μg/ml, with 100 μl per well, and incubated at either at 4 °C overnight or at 37 °C for 2 h. After washing, plates were blocked with 5% non-fat milk in PBS at 37 °C for 60 mins. Subsequently, 100 μl serially diluted anti-sera or purified antibody were added and incubated at 37 °C for 1.5 h. Plates were then washed and incubated with either goat anti-human IgG with HRP (1:10000 dilution, Cat#: 109-035-088, Jackson ImmunoResearch) or goat anti-llama IgG (H + L) secondary antibody with HRP (1:10000 dilution, Cat#: NB7242, Novus) at 37 °C for 1 h. After this incubation, the 3,3′,5,5′-Tetramethylbenzidine (TMB, Sigma) substrate was added and allowed to react at 37 °C for 10 mins. The reaction was terminated by adding 10 μl of 0.2 M H2SO4. Optical densities were measured at 450 nm using the Infinite 200 instrument (Tecan, Ramsey, MN, USA). Antibody titers were determined as the highest dilution at which the sample generated an optical density readout at least 2.1-fold higher than the control serum sample at the same dilution.

Construction of a phage library displaying VHH antibody

A VHH phage library was established with certain modifications made to a previously documented method[35]. In brief, peripheral blood mononuclear cells (PBMCs) were isolated from 100 ml blood obtained from the immunized alpaca, employing a lymphocyte separation solution (GE Ficoll-Paque Plus, Cat#: 17-1140-02). RNA was extracted and reverse transcribed into cDNA, following the TRIzol kit's instructions, utilizing oligo (dT) and random hexamers as primers. Subsequently, the alpaca VHH gene was amplified using specific primer combinations and then cloned into the phV1 phagemid plasmid (Abrev, Ltd., Nanjing, China) for subsequent transformation into TG1 bacteria.

Panning VHH phage library

Affinity selection of CD4-binding recombinant phages was performed using an enrichment protocol, with modifications adapted from a previously described method[36]. Specifically, VHH-phagemid-transformed bacteria were rescued using M13KO7 helper phage (Cat#: 18311019, Invitrogen) and then precipitated using PEG/NaCl. The phage VHH antibody library underwent three rounds of enrichment by incubation with 50 μg/ml of CD4-His protein. The enriched phage pool was subsequently eluted, transformed, and monoclonal phages were selected for evaluation via phage ELISA using CD4 as the target protein. For Phage ELISA, 96-well plates (Cat#: 9018, Corning) were coated with 200 ng of CD4-His protein in a coating buffer (pH 9.6) and incubated at 4 °C overnight. The plates were then blocked for 1 hour at 37 °C with blocking buffer (3% BSA in PBST), followed by incubation with library phages or single clone phages in bacterial supernatants at 4 °C for 1.5 hours. After washing, anti-M13 bacteriophage antibody with HRP (1:10000 dilution, Cat#: 11973-MM05T-H, Sino Biological) was added and incubated at 37 °C for 1 h. Subsequently, 3,3′,5,5′-Tetramethylbenzidine (TMB, Sigma) substrate was added and allowed to react at 37 °C for 10 min, with the reaction being quenched by adding 10 μl of 0.2 M H2SO4. Optical densities were measured at 450 nm using the Infinite 200 instrument (Tecan, Ramsey, MN, USA). Clones exhibiting a readout at 450 nm greater than 0.5 were selected for sequencing.

Construction and expression of VHH antibody library

The enriched VHH phage library underwent PCR amplification to yield VHH gene fragments, which were subsequently cloned into the prokaryotic expression vector pComb3X. This step resulted in the establishment of a prokaryotic expression VHH antibody library. The library was induced to express VHH antibodies using IPTG, and the bacterial supernatants were assessed using ELISA with CD4 as the target protein. Positive clones were identified by CD4/Blank ratios > 5.0, and the corresponding bacterial clones were sequenced. Among these colonies, a total of 1920 monoclonal colonies were randomly selected. The bacterial supernatants from these colonies were evaluated for their potential to neutralize HIV infection.

VHH-huFc4 (Nb-Fc) or Ibalizumab eukaryotic expression

To enhance the function and stability of VHH antibodies, the *Fc4* gene (CH2-CH3) of human monoclonal antibody was fused with VHH gene and cloned into the pVAX1 eukaryotic expression vector. This approach aimed to improve the half-life, Fc-based function, and purification of the VHH antibody. The resultant constructed VHH-huFc-pVAX1 was then transfected into 293 F cells to produce VHH-huFc4 (Nb-Fcs, ~80 kDa) antibody. Following expression, the antibodies were purified using Protein G (Cat#:20399, Thermo Scientific). Meanwhile, Ibalizumab (~ 150 kDa) was constructed within the pVAX1 vector, following the published gene sequence, and was likewise expressed in 293 F cells as Nb-Fc for further analysis.

Expression and purification of trimeric Nb457

To improve the activity of Nb457, we constructed Nb457 with trimeric Nbs configurations (Nb_{457}-Nb_{HSA}-$Nb_{457,}$ ~ 40 kDa) wherein $(GGGGS)_3$ linkers were introduced between Nbs in trimeric forms as our previously reported[15]. The specific nanobody targeting Human Serum Albumin (HSA), Nb_{HSA}, was developed through immunization of an alpaca with HSA[15]. To facilitate protein purification, a 6 x His-tag was fused to the C terminus of the Nbs of trimeric configuration.

Subsequently, these trimeric Nb457 were cloned into the pcDNA3.4 eukaryotic expression vector (Invitrogen). The vectors containing the engineered trimeric Nbs were then transfected into 293 F cells for the production. To isolate and purify the trimeric Nb457 fused with the His-tag, we employed Ni-NTA affinity chromatography (Cat.# R901100, Thermo Fisher Scientific).

Affinity determination by bio-layer interferometry (BLI)

The affinity of antibodies was assessed employing a ForteBio OctetRED 96 BLI system (Molecular Devices ForteBio LLC, Fremont, CA), maintaining a shaking rate of 1000 rpm at 25 °C, in accordance with previously established protocols outlined in ref. 15. To quantify the affinity of nanobodies (Nbs) bearing a human Fc tag, Nb-Fcs were immobilized onto anti-human Fc (AHC) biosensors (Cat# 18-5060, Fortebio) within a kinetic buffer (PBS, 0.02% (v/v) Tween-20, pH 7.0) for a duration of 200 s. Subsequently, baseline equilibration was carried out for an additional 180 s within the same kinetic buffer. The association phase with CD4 was conducted using a three-fold dilution series spanning concentrations from 300 nM to 0.4 nM, followed by a dissociation phase lasting 180 s. After each binding cycle, biosensors were regenerated by three brief pulses of 5 s each with 100 mM pH 2.7 glycine-HCL buffer. Data analysis encompassed baseline subtraction, and fitting was performed employing a 1:1 binding model in conjunction with the ForteBio data analysis software. To elucidate the kinetic parameters, including the dissociation constant (KD), association rate constant (Ka), and dissociation rate constant (Kd), a global fitting approach was applied to all collected data.

HIV-1 neutralization assay

The Global Panel HIV-1 Env clones were acquired from the NIH AIDS Reagent Program (Cat# 12670)[8]. Additionally, a set of 35 Env clones was generated by us or generously provided by our collaborator (H Shang, China Medical University, Shenyang, China)[37]. To assess the efficacy and breadth of various anti-sera or neutralizing nanobodies or antibodies, a luciferase-based assay was performed using a standard inoculum consisting of 200 $TCID_{50}$ of each pseudovirus as previously described[8], in GHOST(3)-X4R5 (Cat# 3942, NIH AIDS Reagent Program). The neutralizing activity of each anti-serum, nanobodies or antibodies was tested in duplicate with a 3-fold serial dilution. The half-maximal inhibitory concentration (IC_{50}), the eightieth percentile inhibitory concentration (IC_{80}) and the ninetieth percentile inhibitory concentration (IC_{90}) of each Nb or antibody were calculated to determine anti-HIV-1 potency. For live HIV-1 neutralization assessments, we conducted the assay using TZM-bl cells (Cat# 8129, NIH AIDS Reagent Program) and a standardized viral inoculum of 200 $TCID_{50}$.

In vivo evaluation of Nbs inhibition of HIV infection in NDG-HuPBL mice

HIV-infected immunodeficient NOD.CB17-PrkdcscidIl2rgtm1/Bcgen (NDG) mice were established following our previous protocol[33]. In brief, 1.0×10^6 to 1.5×10^7 human peripheral blood lymphocyte (HuPBL) were injected intraperitoneally into 4–6-week-old of female NDG mice (Biocytogen Co., Ltd., China); blood samples from NDG-HuPBL mice collected after two weeks were subjected to flow cytometry to determine the percentage of human $CD45^+$, $CD3^+$, $CD4^+$ and $CD8^+$. NDG-HuPBL Mice with a proportion of human $CD45^+$ cells exceeding 5% were selected for the study. NDG-HuPBL mice were challenged with 10 ng p24 of live of HIV_{CH058}, originating from a transmitted/founder virus (generously provided by the NIH), known to be a tier 2 virus, and exhibiting resistance to most antibody neutralization[28]. The infected NDG-HuPBL mice ($n = 4$, female) were treated with 400 μg of nanobodies per mouse via intraperitoneal (*i.p.*) or subcutaneous (*s.c.*) injection at specified time points. Control nanobodies were administered to infected mice following the same time intervals. Sample Collection and Analysis Blood samples were collected at designated time points for various analyses. The concentration of nanobodies in sera was determined using ELISA. Viral load was monitored by quantitative polymerase chain reaction (qPCR). Ultimately, mice were sacrificed for comprehensive detection of infected cells throughout the body.

Viral RNA quantification via quantitative reverse transcription polymerase chain reaction (qRT-PCR)

Viral RNA extraction was accomplished using the QIAamp viral RNA mini kit (Qiagen). The extracted RNA underwent reverse transcription, yielding 20 μl of complementary DNA (cDNA). The reverse transcription process was executed employing the RT-PCR Prime Script Kit (Takara). This resulting cDNA served as the template for subsequent quantitative RT-PCR (qRT-PCR) analysis. For each qRT-PCR reaction, 8 μl of cDNA was combined with TaqMan Universal PCR Master Mix (Life Technologies), a TaqMan probe (5′-FAM – CTCTCT CCTTCT AGCCTC – MGB-3′), and primers that were bespoke to target the *P17* gene of HIV-1 (Forward: 5′-TACTGA CGCTCT CGCACC-3′; Reverse: 5′-TCTCGA CGCAGG ACTCG-3′). Amplification was conducted in triplicate on an Eppendorf Realplex4 Mastercycler (Eppendorf) under the following cycling conditions: an initial cycle at 50 °C for 2 min, followed by a cycle at 95 °C for 10 min, and subsequently 40 cycles at 95 °C for 15 s and 60 °C for 1 min. Viral titer quantification was determined by referencing the samples against a standard curve generated using RNA extracted from a serially diluted reference viral stock. The assay's limit of detection for live HIV-1 was established at 1000 copies per ml, attesting to its sensitivity and precision.

Flow cytometry analysis

Blood samples were collected from the facial veins of mice into Eppendorf tubes containing 50 μl of anti-coagulant (0.5 M EDTA). Subsequently, the samples were centrifuged at $1150 \times g$ for 5 min using a microcentrifuge. The resulting plasma was carefully preserved for future analyses, while the cellular pellets were resuspended in 2 ml of 1x RBC lysis buffer (BD Bioscience). Following resuspension, the samples were incubated on ice for 10 min to facilitate the removal of red blood cells. Following lysis, the cells underwent a secondary centrifugation step at $1150 \times g$ for 5 min at room temperature. The cell pellets were then subjected to immunostaining for a duration of 60 min at 4 °C using a cocktail comprising 100 μl, which included 2 μl of anti-human CD3-Pacific Blue (Cat# 300442/UCHT1, Biolegend), 2 μl of anti-human CD4-PerCP-Cy5.5 (Cat# 317428/OKT4, Biolegend), 2 μl of anti-human CD8-PE antibodies (Cat# 344706/SK1, Biolegend), and 2 μl of anti-human CD45 PE/Cy7 (Cat# 304016/H130, Biolegend). After staining, the samples were meticulously washed with phosphate-buffered saline (PBS) supplemented with 2% fetal bovine serum (wash buffer). Subsequently, they were centrifuged at $800 \times g$ in a microcentrifuge for 5 min. The pelleted cells were resuspended in 300 μl of wash buffer and then subjected to analysis. Flow cytometry analysis was performed utilizing a NovoCyte FACS system (Agilent), with data analyzed using FlowJo software version 10.2. Initial gating of samples was carried out based on the expression of human CD45, followed by further analysis of T cell subsets, characterized by the CD3, CD4, and CD8 markers within this gated subset.

Immunofluorescence staining of HIV-infected cells in tissues

Tissues, including the spleen and other tissues, were promptly immersed in 10% neutral buffered formalin for a 24-hour period to ensure optimal fixation. Following fixation, the tissues underwent a transition into 70% ethanol and were subsequently embedded in paraffin. Tissue section with 4 μm in thickness were employed for the Immunofluorescence staining of HIV-p24 using the anti-P24 nanobody fused with rabbit Fc (NbP24-rFc) (Cat# AR0358, Abrev, China), as

previously documented[38]. Confocal imaging of these tissue sections was captured using the FV3000 confocal microscope (Olympus), facilitating the acquisition of high-resolution images.

Expression and purification of D1-D2 domain of CD4 protein for crystal structural analysis

The recombinant D1-D2 domain of the CD4 protein was expressed using the Bac-to-Bac baculovirus system. The pFastBac1 plasmid, containing the gp67 signal peptide and a C-terminal 6×His tag, was transfected into Sf9 insect cells with Lipofectamine 3000 Reagent (Invitrogen), resulting in the generation of recombinant baculoviruses. Subsequently, these baculoviruses were amplified within Sf9 cells, and after 48 h post-infection, cell culture supernatants containing the secreted D1-D2 protein were collected. Purification of the D1-D2 protein was conducted through Ni-NTA resin (GE Healthcare) to selectively eliminate nonspecific contaminants. The target protein was eluted using an elution buffer consisting of 20 mM Tris-HCl, 150 mM NaCl, and 300 mM imidazole at pH 7.5. To further improve the purity, a final purification step was conducted using Superdex 200 chromatography (GE Healthcare, USA). The purified proteins were stored in a buffer solution containing 20 mM Tris-HCl and 150 mM NaCl at pH 7.5.

Expression and purification of Nb457 for crystal structural analysis

The VHH gene encoding Nb457 was amplified via PCR and subsequently cloned into the pET22b vector using Nco I and Xho I restriction sites. Following cloning, the recombinant plasmids were introduced into *Escherichia coli* BL21 (DE3) cells. Specifically, the bacterial culture was nurtured in LB medium at 37 °C until reaching an optical density at 600 nm (OD_{600}) of 0.6. Protein expression was initiated by the addition of isopropyl-D-1-thiogalactopyranoside (IPTG) to a final concentration of 0.5 mM, and the bacterial culture was incubated at 16 °C for 20 h. The bacterial cells were harvested by centrifugation at 4500 rpm for 15 min and subsequently re-suspended and homogenized in a lysis buffer (20 mM Tris-HCl, 150 mM NaCl, pH 7.5, 10 mM imidazole) utilizing ultrasonication. Following bacterial lysis, the lysate was centrifuged at 18,000 rpm for 30 minutes, and the resulting supernatant was applied to Ni-NTA resin (GE Healthcare, USA) for protein purification. The proteins were eluted with a buffer containing 300 mM imidazole, 20 mM Tris-HCl, and 150 mM NaCl. Further purification was conducted using Superdex 200 chromatography (GE Healthcare, USA) to ensure the highest level of protein purity for subsequent crystal structural analysis.

Crystallization, structural determination and data acquisition

The D1D2-Nb457 complexes were generated by mixing the components at a 1:1.5 molar ratio (30 mg/ml), followed by incubation at 4 °C overnight. Crystals of the complexes were grown using the vapor-diffusion sitting-drop method at 16 °C, reaching their final size within 3 days in a crystallization solution consisting of 0.1 M sodium cacodylate trihydrate at pH 6.8 and 1.4 M sodium acetate trihydrate. For data collection, a single crystal was mounted on a nylon loop and flash-cooled with a nitrogen gas stream at 100 K. Diffraction data for D1D2-Nb457 were collected at Shanghai Synchrotron Radiation Facility (SSRF) on BL19U1 using a wavelength of 0.97853 Å. Data processing and scaling were carried out using the HKL3000 package[39]. Molecular replacement (MR) utilized the PHASER program with reference structures (PDB: 1CDH and 5LHR)[40], and model refinement was performed within the modified experimental electron density using COOT and PHENIX[41,42]. Structural figures were created with PyMOL (http://www.pymol.org), and epitope and paratope residues, along with their interactions, were identified using PISA[43] (http://www.ebi.ac.uk/pdbe/prot_int/pistart.html) at the European Bioinformatics Institute and LigPlot+ 2.2[44].

Assessment of Nb457's influence on CD4 binding to cell surface MHC-II

The interaction between CD4 protein and MHC-II protein on the surface of Daudi cells was examined following established protocols[45]. CD4 protein fused with rabbit Fc (CD4-rFc) was prepared at varying concentrations (ranging from 0.01 ug/ml to 2.2 ug/ml). Subsequently, 1 × 10 ^ 6 Daudi cells were separately incubated with CD4-rFc at 4 °C for 30 min. Following incubation, cells were subjected to two washes with PBS and subsequently incubated at 4 °C for 20 min with Alexa Fluor® 488 AffiniPure Goat Anti-Rabbit IgG (H + L) (1:500 dilution) (cat# 128-545-160, Jackson ImmunoResearch). After washes, flow cytometry was utilized for subsequent analysis.

Based on the experimental findings, the linear concentration range for the binding of CD4-rFc to MHC-II on the surface of Daudi cells was determined. CD4-rFc protein, at the concentration established within the linear range, was then incubated with nanobodies or antibodies at 20-fold concentrations at 4 °C for 2 h. Subsequently, 1 × 10 ^ 6 Daudi cells were transferred to round-bottomed well plates, centrifuged at 800 × g, washed once with PBS, and then incubated with the mixture of the aforementioned protein and antibodies at 4 °C for 30 min. After washes, cells were incubated at 4 °C for 20 min with Alexa Fluor® 488 AffiniPure Goat Anti-Rabbit IgG (H + L) (1:500 dilution) (cat# 128-545-160, Jackson ImmunoResearch). Following washes, flow cytometry was employed for subsequent analysis.

Model construction

To facilitate subsequent molecular dynamics simulations, we crafted three pivotal molecular structures: Nb_{457}-Fc, Nb_{457}-Nb_{HSA}-Nb_{457}, and the HIV-1_{CH058} gp120. Our foundational structure for Nb_{457} (PDB: 8W90) was previously elucidated in this study, and we complemented this with the acquisition of the Fc structure from the Protein Data Bank (PDB: 5dk3). These templates underwent modeling within the MODELLER framework using homology modeling techniques, resulting in a model of the Nb_{457}-Fc structure. Leveraging the conspicuous amino acid sequence homology between Nb_{457} and Nb_{HSA}, we conducted precise homology modeling using SWISS-MODEL[46], culminating in the formation of the Nb_{HSA} structure. Subsequently, we harnessed MODELLER once more, orchestrating the integration of both Nb_{457} and Nb_{HSA} structures, thus achieving the comprehensive Nb_{457}-Nb_{HSA}-Nb_{457} configuration. Significantly, to address the formidable challenge arising from substantial sequence disparities between extant gp120 structures and the unique variant structure of HIV-1_{CH058} gp120, which was evaluated in our live HIV-1 neutralization assay, we harnessed the advanced capabilities of AlphaFold2[47], a state-of-the-art deep learning methodology, to predict the intricate architecture of our target gp120 derived from HIV-1_{CH058}. This approach provided a model to be used in our simulations, recognizing the potential uncertainties inherent in computational predictions.

Molecular dynamics simulations

To gain insight into the mechanisms underlying the actions of Nb_{457}-Fc and Nb_{457}-Nb_{HSA}-Nb_{457}, we established three distinct systems: one devoid of antibodies (comprising only CD4+gp120), another incorporating Nb_{457}-Fc (denoted as Nb_{457}-Fc+CD4+gp120), and a third encompassing Nb_{457}-Nb_{HSA}-Nb_{457} (referred to as Nb_{457}-Nb_{HSA}-Nb_{457} + CD4+gp120). The preparation of these systems was meticulously executed using CHARMM-GUI. Subsequent molecular dynamics (MD) simulations were conducted on each system, employing the GROMACS 2023 package. The force field utilized for all systems was CHARMM36m, accompanied by the TIP3P water model[48]. Neutralization of protein charges was achieved by introducing a 150 mM salt concentration of sodium chloride. The MD simulations were carried out within periodic boundary conditions, employing the NpT ensemble, with temperature maintained at 303 K and pressure set to 1 bar. Prior to the commencement of MD

simulations, all systems underwent a 5000-step energy minimization protocol. Subsequently, MD simulations, with position restraints applied to the protein backbone atoms, were executed for 125 ps, serving as a pre-equilibration step before the 500 ns production MD simulations. To assess the dynamics of the systems, we conducted Root Mean Square Fluctuation (RMSF) analysis, hydrogen bond analysis, and cluster analysis, utilizing built-in programs within GROMACS, namely rmsf, hbond, and cluster.

Hydrogen bond analysis

To analyze the influence of Nb_{457}-Fc and Nb_{457}-Nb_{HSA}-Nb_{457} on the CD4-gp120 interaction, we conducted an in-depth examination of main-chain hydrogen bonds between CD4 and gp120. Utilizing the hbond analysis module in GROMACS, we generated time-dependent profiles of main-chain hydrogen bond occurrences within each system. Subsequently, employing cluster analysis within GROMACS, we identified the conformation exhibiting the highest frequency as the most probable configuration. The corresponding PDB file for this configuration was then imported into Chimera for comprehensive visualization and further analysis, specifically focusing on the main-chain hydrogen bonds formed[49].

PBMC culture and stimulation

PBMCs were thawed and treated with Universal Nuclease (Cat# 20156ES25, Yeasen, China) at a final concentration of 12 U/ml for 2 h at 37 °C. Subsequently, cells were gently washed with complete culture medium (RPMI 1640 medium, Life Technologies). The cells were then incubated with nanobodies or antibodies at a concentration of 20 ug/ml at 37 °C. The culture medium used was RPMI 1640 supplemented with 10% FBS and 100 U/ml of IL-2, with or without 1×PHA (Cat# 00-4977-93, Ebioscience). All cultures were maintained at 37 °C in a 5% CO_2 incubator.

Intracellular cytokine analysis

Following 40 h of culture, 5 μg/ml Brefeldin A (Cat# 2031560, BioGems) was added into the treated PBMC. After an additional 8 h, cells were harvested, and cytokine levels were assessed. Extracellularly, cells were stained with fluorescently labeled antibodies, including anti-CD3 Pacific Blue (UCHT1, Biolegend), anti-CD4 PE-Cy7 (OKT4, Biolegend), anti-CD8 PE (SK1, Biolegend), and Fixable Viability dye (Cat# 65-0866-14, Ebioscience). Incubation was conducted for 20 min at 4 °C. Subsequently, cells were washed, fixed, and permeabilized using BD Cytofix/Cytoperm solution (Cat# 554714, BD Biosciences) following the manufacturer's instructions. Intracellular staining was performed for anti-TNFα BV786 (Mab11, Biolegend), anti-IL-2 APC (MQ1-17H12, BD), and anti-IFN-γ FITC (4 S.B7, BD). Following washes, samples were analyzed by flow cytometry.

Cell proliferation and activation assessment

After three days of culture, cells were harvested, and extracellular staining was performed using anti-CD4 PE-Cy7 (OKT4, Biolegend), anti-CD8 PE (SK1, Biolegend), and Fixable Viability dye (Cat# 65-0866-14, Ebioscience). Incubation was carried out for 20 min at 4 °C. Following washes, cells were fixed with BD permeabilization buffer and subjected to intracellular staining using anti-Ki67 Pacific blue (RUO, Biolegend) for 30 min at 4 °C. After washes, samples were analyzed using flow cytometry.

Pharmacokinetics (PK) of Nb457 and Ibalizumab in vivo

Purified Nb457 nanobodies were administered to NDG-HuPBL (Biocytogen Co., Ltd., China) via intraperitoneal (*i.p.*) or subcutaneous (*s.c.*) injection with 400 μg per mouse (average 20 mg/kg). The quantification of Nb457 or control antibodies levels in serum was accomplished by ELISA. To determine the half-life (T1/2) of Nb457 and Ibalizumab, we applied the equation $T1/2 = \ln(2)/k$, where 'k' represents the rate constant, reciprocally expressed in units corresponding to the *x*-axis time, derived from a one-phase decay equation using GraphPad software.

Statistical analysis

Graphs were generated using GraphPad Prism 5.01 software (GraphPad) or OriginPro 8.5 software (OriginLab). One-way or two-way ANOVA was performed for group comparisons. $P < 0.05$ was considered as statistically significant with mean ± SEM or mean ± SD or median + range.

Study approval

The experimental procedures conducted within this research were approved by the Center for Public Health Research, Medical School, Nanjing University. All of the mice were treated in accordance with the China Ethical Guidelines for the Welfare of Laboratory Animals (GB 14925-2010). All protocols pertaining to animals infected with HIV were executed within Biosafety Level 3 animal facilities, aligning with the recommendations for the ethical care and utilization of animals as specified by the Institutional Review Board of Wuhan Institute of Virology, and performed in accordance with the Guidelines of the Hubei Laboratory Animal Science Association (Approval number: WIVA11202202). All authors declare their adherence to the publishing ethics in the conduct and dissemination of this study.

Reporting summary

Further information on research design is available in the Nature Portfolio Reporting Summary linked to this article.

Data availability

All data are available in the main text or the supplementary materials. The crystal structure of D1-D2 of CD4 protein with Nb457 was deposited in the Protein Data Bank (PDB) with accession code 8W90. Source data are provided with this paper.

References

1. Van de Perre, P. et al. Eliminating postnatal HIV transmission in high incidence areas: need for complementary biomedical interventions. *Lancet* **397**, 1316–1324 (2021).
2. Gupta-Wright, A. et al. Virological failure, HIV-1 drug resistance, and early mortality in adults admitted to hospital in Malawi: an observational cohort study. *Lancet HIV* **7**, e620–e628 (2020).
3. Gupta, R. K. et al. HIV-1 drug resistance before initiation or re-initiation of first-line antiretroviral therapy in low-income and middle-income countries: a systematic review and meta-regression analysis. *Lancet Infect. Dis.* **18**, 346–355 (2018).
4. Haynes, B. F., Burton, D. R. & Mascola, J. R. Multiple roles for HIV broadly neutralizing antibodies. *Sci. Transl. Med.* **11**, eaaz2686 (2019).
5. Caskey, M., Klein, F. & Nussenzweig, M. C. Broadly neutralizing anti-HIV-1 monoclonal antibodies in the clinic. *Nat. Med.* **25**, 547–553 (2019).
6. Emu, B. et al. Phase 3 study of ibalizumab for multidrug-resistant HIV-1. *N. Engl. J. Med.* **379**, 645–654 (2018).
7. Blair, H. A. Ibalizumab: a review in multidrug-resistant HIV-1 infection. *Drugs* **80**, 189–196 (2020).
8. Wu, X. et al. Tandem bispecific neutralizing antibody eliminates HIV-1 infection in humanized mice. *J. Clin. Invest.* **128**, 2239–2251 (2018).
9. Niu, M. et al. Tandem bispecific antibody prevents pathogenic SHIVSF162P3CN infection and disease progression. *Cell Rep.* **36**, 109611 (2021).
10. Harmsen, M. M. & De Haard, H. J. Properties, production, and applications of camelid single-domain antibody fragments. *Appl. Microbiol. Biotechnol.* **77**, 13–22 (2007).
11. Hamerscasterman, C. et al. Naturally-occurring antibodies devoid of light-chains. *Nature* **363**, 446–448 (1993).

12. Jovcevska, I. & Muyldermans, S. The therapeutic potential of nanobodies. *Biodrugs* **34**, 11–26 (2020).
13. Muyldermans, S. Applications of Nanobodies. *Annu Rev Anim Biosci.* **9**, 401–421 (2021).
14. Ji, M. et al. Inhibition of SFTSV replication in humanized mice by a subcutaneously administered anti-PD1 nanobody. *EMBO Mol. Med.* **16**, 575–595 (2024).
15. Wu, X. et al. A potent bispecific nanobody protects hACE2 mice against SARS-CoV-2 infection via intranasal administration. *Cell Rep.* **37**, 109869 (2021).
16. Wu, X. et al. Short-term instantaneous prophylaxis and efficient treatment against SARS-CoV-2 in hACE2 mice conferred by an intranasal nanobody (Nb22). *Front. Immunol.* **13**, 865401 (2022).
17. Koenig, P. A. et al. Structure-guided multivalent nanobodies block SARS-CoV-2 infection and suppress mutational escape. *Science* **371**, eabe6230 (2021).
18. Chen, F., Liu, Z. & Jiang, F. Prospects of neutralizing nanobodies against SARS-CoV-2. *Front. Immunol.* **12**, 690742 (2021).
19. Scully, M. et al. Caplacizumab treatment for acquired thrombotic thrombocytopenic purpura. *N. Engl. J. Med.* **380**, 335–346 (2019).
20. Zheng, F. et al. Applications of nanobodies in brain diseases. *Front. Immunol.* **13**, 978513 (2022).
21. Traenkle, B. et al. Single-domain antibodies for targeting, detection, and in vivo imaging of human CD4(+) cells. *Front. Immunol.* **12**, 799910 (2021).
22. Duan, L. W. et al. A non-canonical binding interface in the crystal structure of HIV-1 gp120 core in complex with CD4. *Sci. Rep.* **7**, 46733 (2017).
23. Kwong, P. D. et al. Structure of an HIV gp120 envelope glycoprotein in complex with the CD4 receptor and a neutralizing human antibody. *Nature* **393**, 648–659 (1998).
24. Freeman, M. M. et al. Crystal structure of HIV-1 primary receptor CD4 in complex with a potent antiviral antibody. *Structure* **18**, 1632–1641 (2010).
25. Yin, Y., Wang, X. X. & Mariuzza, R. A. Crystal structure of a complete ternary complex of T-cell receptor, peptide-MHC, and CD4. *Proc. Natl Acad. Sci. USA* **109**, 5405–5410 (2012).
26. deCamp, A. et al. Global panel of HIV-1 Env reference strains for standardized assessments of vaccine-elicited neutralizing antibodies. *J. Virol.* **88**, 2489–2507 (2014).
27. Zhou, P. et al. Broadly resistant HIV-1 against CD4-binding site neutralizing antibodies. *Plos Pathog.* **15**, e1007819 (2019).
28. Lucas, J. et al. Identification of early-induced broadly neutralizing activities against transmitted founder HIV strains. *Aids* **37**, 43–49 (2023).
29. Huang, Y. X. et al. Engineered bispecific antibodies with exquisite HIV-1-neutralizing activity. *Cell* **165**, 1621–1631 (2016).
30. Pace, C. S. et al. Bispecific antibodies directed to CD4 domain 2 and HIV envelope exhibit exceptional breadth and picomolar potency against HIV-1. *Proc. Natl Acad. Sci. USA* **110**, 13540–13545 (2013).
31. Walsh, S. R. & Seaman, M. S. Broadly neutralizing antibodies for HIV-1 prevention. *Front. Immunol.* **12**, 712122 (2021).
32. Kwong, P. D., Mascola, J. R. & Nabel, G. J. Broadly neutralizing antibodies and the search for an HIV-1 vaccine: the end of the beginning. *Nat. Rev. Immunol.* **13**, 693–701 (2013).
33. Wu, X. et al. A single-domain antibody inhibits SFTSV and mitigates virus-induced pathogenesis in vivo. *JCI insight* **5**, e136855 (2020).
34. Wu, X. et al. Induction of neutralizing antibodies by human papillomavirus vaccine generated in mammalian cells. *Antib. Ther.* **2**, 45–53 (2019).
35. Baral, T. N., MacKenzie, R. & Arbabi Ghahroudi, M. Single-domain antibodies and their utility. *Current protocols in immunology/edited by John E. Coligan...* [et al.] **103**, Unit 2 17, https://doi.org/10.1002/0471142735.im0217s103 (2013).
36. Jahnichen, S. et al. CXCR4 nanobodies (VHH-based single variable domains) potently inhibit chemotaxis and HIV-1 replication and mobilize stem cells. *Proc. Natl Acad. Sci. USA* **107**, 20565–20570 (2010).
37. Shang, H. et al. Genetic and neutralization sensitivity of diverse HIV-1 env clones from chronically infected patients in China. *J. Biol. Chem.* **286**, 14531–14541 (2011).
38. Wu, X. et al. Brain invasion by CD4(+) T cells infected with a transmitted/founder HIV-1BJZS7 during acute stage in humanized mice. *J. NeuroImmune Pharmacol. J. Soc. NeuroImmune Pharmacol.* **11**, 572–583 (2016).
39. Minor, W., Cymborowski, M., Otwinowski, Z. & Chruszcz, M. HKL-3000: the integration of data reduction and structure solution - from diffraction images to an initial model in minutes. *Acta Crystallogr. Sect. D. -Struct. Biol.* **62**, 859–866 (2006).
40. Mccoy, A. J. et al. Phaser crystallographic software. *J. Appl. Crystallogr.* **40**, 658–674 (2007).
41. Adams, P. D. et al. PHENIX: a comprehensive Python-based system for macromolecular structure solution. *Acta Crystallogr. Sect. D. -Struct. Biol.* **66**, 213–221 (2010).
42. Emsley, P., Lohkamp, B., Scott, W. G. & Cowtan, K. Features and development of Coot. *Acta Crystallogr. Sect. D. -Biol. Crystallogr.* **66**, 486–501 (2010).
43. Krissinel, E. & Henrick, K. Inference of macromolecular assemblies from crystalline state. *J. Mol. Biol.* **372**, 774–797 (2007).
44. Laskowski, R. A. & Swindells, M. B. LigPlot+: multiple ligand-protein interaction diagrams for drug discovery. *J. Chem. Inf. Modeling* **51**, 2778–2786 (2011).
45. Doyle, C. & Strominger, J. L. Interaction between CD4 and class II MHC molecules mediates cell adhesion. *Nature* **330**, 256–259 (1987).
46. Waterhouse, A. et al. SWISS-MODEL: homology modelling of protein structures and complexes. *Nucleic Acids Res.* **46**, W296–W303 (2018).
47. Jumper, J. et al. Highly accurate protein structure prediction with AlphaFold. *Nature* **596**, 583–589 (2021).
48. Huang, J. et al. CHARMM36m: an improved force field for folded and intrinsically disordered proteins. *Nat. Methods* **14**, 71–73 (2017).
49. Sanner, M. F., Olson, A. J. & Spehner, J. C. Reduced surface: an efficient way to compute molecular surfaces. *Biopolymers* **38**, 305–320 (1996).

Acknowledgements

This work was supported by the National Science Foundation of China (NSFC) (No.32370988, 31970149 and U22A20335), the Major Research and Development Project (2018ZX10301406), Research Foundation of JiangSu Commission Health project (Grant# ZDA2020014), the National Key Research and Development Program (2023YFC2306600), the Emergency Prevention and Control Capacity Program for New Severe Infectious Diseases of National Institute for Viral Disease Control and Prevention, and the 135 Strategic Program of Chinese Academy of Sciences.

Author contributions

X. Wu and Linjing Zhu conducted most experiments, analyzed the data and wrote the draft manuscript. X. Wang, S.Y. and Y.W. conducted the structural analysis. R.W. and L. Zhang provided technical assistance and conducted the experiments related with pseudovirus neutralization. F.N., M.Y., P.Y., M.L., Y. Li, Q.H., Y. Liu evaluate the efficacy of Nbs against live HIV-1 virus in vitro or in vivo. M.A., B.Z. and P.Z. conducted the molecular dynamics simulation analysis. J.X., Lin Zhu and C.Y. evaluated Nbs against viral infection. X. Wu, Linjing Zhu, B.H., C.C., L.S., S.G., J.H., D.Z., Y. Liu H.W., provided technical assistance and did most experiments. X. Wu and Z.W. designed the study, monitored and financially supported the study and revised the manuscript. All authors critically reviewed the draft manuscript and approved the final version.

Competing interests
The authors declare no competing interests.

Additional information
Supplementary information The online version contains supplementary material available at https://doi.org/10.1038/s41467-024-51414-6.

Correspondence and requests for materials should be addressed to Zhiwei Wu, Linqi Zhang, Yaxin Wang, Yalan Liu or Xilin Wu.

Peer review information *Nature Communications* thanks the anonymous reviewers for their contribution to the peer review of this work. A peer review file is available.

[1]Center for Public Health Research, Medical School, Nanjing University, Nanjing, P.R. China. [2]Jiangsu Key Laboratory of Molecular Medicine, Medical School, Nanjing University, Nanjing, P.R. China. [3]Abrev Biotechnology Co. Ltd., Nanjing, P.R. China. [4]Frontiers Science Center for Synthetic Biology (Ministry of Education), Tianjin Key Laboratory of Function and Application of Biological Macromolecular Structures, School of Life sciences, Tianjin University, Tianjin, P.R. China. [5]State Key Laboratory of Virology, Wuhan Institute of Virology, Center for Biosafety Mega-Science, Chinese Academy of Sciences, Wuhan, P.R. China. [6]Savaid Medical School, University of Chinese Academy of Sciences, Beijin, P.R. China. [7]State Key Laboratory of Coordination Chemistry, Chemistry and Biomedicine Innovation Center (ChemBIC), School of Chemistry and Chemical Engineering, Nanjing University, Nanjing, Jiangsu, P. R. China. [8]Comprehensive AIDS Research Center, Center for Global Health and Infectious Diseases Research, NexVac Research Center, Center for Infectious Diseases Research, Department of Basic Medical Sciences, School of Medicine, Tsinghua University, Beijing, P.R. China. [9]Department of Infection, Nanjing Hospital Affiliated to Nanjing university of Chinese Medicine, Nanjing, P.R. China. [10]NHC Key Laboratory of Human Disease Comparative Medicine, Beijing Key Laboratory for Animal Models of Emerging and Remerging Infectious Diseases, Institute of Laboratory Animal Science, Chinese Academy of Medical Sciences and Peking Union Medical College, Beijing, P.R. China. [11]MOE Key Laboratory of Model Animals for Disease Study, Medical School, Nanjing University, Nanjing, P.R. China. [12]Life Sciences Institute, Zhejiang University, Hangzhou, Zhejiang, P.R. China. [13]School of Life Sciences, Ningxia University, Yinchuan, Ningxia, P.R. China. [14]State Key Laboratory of Analytical Chemistry for Life Science, Nanjing University, Nanjing, P.R. China. [15]Hubei Jiangxia Laboratory, Wuhan, P.R. China. [16]These authors contributed equally: Linjing Zhu, Bilian Huang, Xiangyao Wang, Fengfeng Ni, Mingjun Ao. ✉e-mail: wzhw@nju.edu.cn; zhanglinqi@tsinghua.edu.cn; wangyaxin@tju.edu.cn; liuyl@wh.iov.cn; xilinwu@nju.edu.cn